Toward understanding the post-collisional evolution of an orogen influenced by convergence at adjacent plate margins; Late Cretaceous-Tertiary thermotectonic history of the Apuseni Mountains

Merten, S.; Matenco, L.C.; Foeken, J.P.T.; Andriessen, P.A.M.

published in
Tectonics
2011

DOI (link to publisher)
10.1029/2011TC002887

document version
Publisher's PDF, also known as Version of record

Toward understanding the post-collisional evolution of an orogen influenced by convergence at adjacent plate margins: Late Cretaceous–Tertiary thermotectonic history of the Apuseni Mountains

S. Merten,[1,2] L. Matenco,[1,3] J. P. T. Foeken,[2,4,5] and P. A. M. Andriessen[1,2]

Received 8 February 2011; revised 12 July 2011; accepted 17 August 2011; published 10 November 2011.

[1] The relationship between syn- to post-collisional orogenic shortening and stresses transmitted from other neighboring plate boundaries is important for understanding the kinematics of mountain belts, but has received little attention so far. The Apuseni Mountains are an example of an orogen in the interference zone between two other subduction systems located in the external Carpathians and Dinarides. This interference is demonstrated by the results of a combined thermochronological and structural field study that quantifies the post-collisional latest Cretaceous–Tertiary evolution. The exhumation history derived from apatite fission track and (U-Th)/He thermochronology indicates that the present-day topography of the Apuseni Mountains originates mainly from latest Cretaceous times, modified by two tectonic pulses during the Paleogene. The latter are suggested by cooling ages clustering around ~45 Ma and ~30 Ma and the associated shortening recorded along deep-seated fault systems. Paleogene exhumation pulses are similar in magnitude (~3.5 km) and are coeval with the final collisional phases recorded in the Dinarides and with part of the Carpathian rotation around the Moesian promontory. These newly quantified Paleogene exhumation and shortening pulses contradict the general view of tectonic quiescence, subsidence and overall sedimentation for this time interval. The Miocene collapse of the Pannonian Basin did not induce significant regional exhumation along the western Apuseni flank, nor did the subsequent Carpathian collision. This is surprising in the overall context of Pannonian Basin formation and its subsequent inversion, in which the Apuseni Mountains were previously interpreted as being significantly uplifted in both deformation stages.

Citation: Merten, S., L. Matenco, J. P. T. Foeken, and P. A. M. Andriessen (2011), Toward understanding the post-collisional evolution of an orogen influenced by convergence at adjacent plate margins: Late Cretaceous–Tertiary thermotectonic history of the Apuseni Mountains, *Tectonics*, *30*, TC6008, doi:10.1029/2011TC002887.

1. Introduction

[2] Current tectonic models generally assume that continental collision coincides with the onset of out-of-sequence deformation at or near the plate boundary, such as backward vergent thrusting [e.g., *Willett and Brandon*, 2002]. It remains to be seen whether the evolution of type examples such as the Alps [e.g., *Schmid et al.*, 1996] can be extrapolated to other orogens, since orogenic shortening depends also on the interplay between syn- and post-collisional shortening and activity at other plate boundaries situated in the vicinity. For instance, the Alpine type example for retro-shear collision [e.g., *Schmid et al.*, 1996] might be laterally discontinuous, since the retro-wedge of the Swiss Alps can also be considered as the fore-wedge of the Dinarides (Alpine subduction polarity versus Dinaridic polarity [e.g., *Laubscher*, 1971; *Kissling et al.*, 2006]). Interaction between different orogens can be studied by means of lithospheric and mantle scale studies (such as subduction-polarities derived from teleseismic mantle tomography [e.g., *Lippitsch et al.*, 2003]), or typically by a combined analysis of exhumation and structural patterns of the syn- and post-collisional stages [e.g., *Batt and Brandon*, 2002; *Kirstein et al.*, 2010].

[3] The Apuseni Mountains in Romania represent such a collisional area derived from the late Early Cretaceous closure of the East Vardar segment of the Neotethys Ocean (or the Transylvanides of *Săndulescu* [1988]; Figure 1). Closure of East Vardar was followed by Late Cretaceous–Miocene

[1]Netherlands Research Centre for Integrated Solid Earth Science, Amsterdam, Netherlands.
[2]Department of Isotope Geochemistry, Faculty of Earth and Life Sciences, VU University, Amsterdam, Netherlands.
[3]Department of Tectonics, Faculty of Earth and Life Sciences, VU University, Amsterdam, Netherlands.
[4]Isotope Geosciences Unit, Scottish Universities Environmental Research Centre, East Kilbride, UK.
[5]Now at Research and Technology Department, Qatar Petroleum, Doha, Qatar.

0278-7407/11/2011TC002887

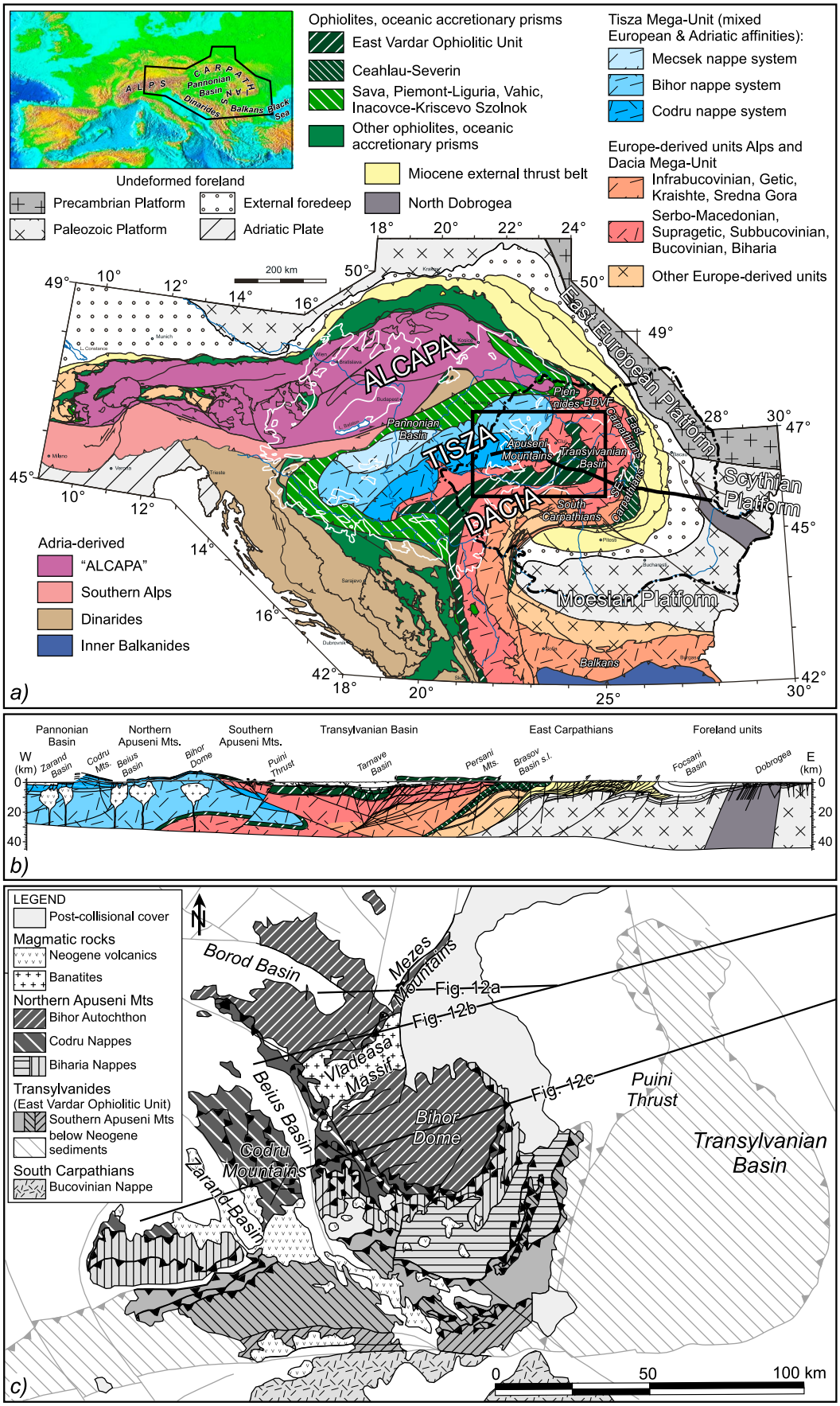
Ophiolites, oceanic accretionary prisms
East Vardar Ophiolitic Unit
Ceahlau-Severin
Sava, Piemont-Liguria, Vahic, Inacovce-Kriscevo Szolnok
Other ophiolites, oceanic accretionary prisms
Tisza Mega-Unit (mixed European & Adriatic affinities):
Mecsek nappe system
Bihor nappe system
Codru nappe system
Europe-derived units Alps and Dacia Mega-Unit
Infrabucovinian, Getic, Kraishte, Sredna Gora
Serbo-Macedonian, Supragetic, Subbucovinian, Bucovinian, Biharia
Other Europe-derived units
Undeformed foreland
Precambrian Platform
Paleozoic Platform
External foredeep
Adriatic Plate
Miocene external thrust belt
North Dobrogea
200 km
ALCAPA
TISZA
DACIA
Pannonian Basin
Apuseni Mountains
Transylvanian Basin
East European Platform
Scythian Platform
Moesian Platform
Balkans
South Carpathians
Adria-derived
"ALCAPA"
Southern Alps
Dinarides
Inner Balkanides
a)
Pannonian Basin
Northern Apuseni Mts.
Southern Apuseni Mts.
Transylvanian Basin
East Carpathians
Foreland units
Zarand Basin
Codru Mts.
Beius Basin
Bihor Dome
Puini Thrust
Tarnave Basin
Persani Mts.
Brasov Basin s.l.
Focsani Basin
Dobrogea
W (km)
E (km)
b)
LEGEND
Post-collisional cover
Magmatic rocks
Neogene volcanics
Banatites
Northern Apuseni Mts
Bihor Autochthon
Codru Nappes
Biharia Nappes
Transylvanides
(East Vardar Ophiolitic Unit)
Southern Apuseni Mts below Neogene sediments
South Carpathians
Bucovinian Nappe
Borod Basin
Mezes Mountains
Fig. 12a
Fig. 12b
Fig. 12c
Vladeasa Massif
Beius Basin
Codru Mountains
Zarand Basin
Bihor Dome
Puini Thrust
Transylvanian Basin
0
50
100 km
c)

Figure 1

activity at two other plate contacts in its vicinity, which closed the Ceahlău-Severin and Sava Oceans of the External Carpathians and Dinarides, respectively [e.g., *Schmid et al.*, 2008] (Figure 1). It is unknown whether activity at these plate contacts is also responsible for the coeval contractional deformations recorded near the East Vardar suture. In addition, the present-day isolated position of the Apuseni Mountains in the intra-Carpathian region is poorly understood in the context of the Miocene–Quaternary tectonic events acting at a more regional Pannonian–Carpathian scale. These events include the Miocene back-arc collapse of the Pannonian Basin and the Pliocene–Quaternary inversion of the entire orogenic and back-arc basin system [e.g., *Tari et al.*, 1999; *Horváth et al.*, 2006; *Pinter et al.*, 2005].

[4] The lack in understanding of the late stage (post-) collisional exhumation history warrants the need of a high-resolution, low-temperature thermochronological study. The apatite fission track (AFT) and apatite (U-Th)/He (AHe) methods are such low-temperature thermochronometers with temperature sensitivities of ~120–60°C (Apatite Partial Annealing Zone (APAZ)) [*Gleadow and Duddy*, 1981] and ~85–40°C (Helium Partial Retention Zone (HePRZ)) [*Wolf et al.*, 1998], respectively. These methods can be used to constrain cooling histories in the upper few kilometers of the Earth's crust [e.g., *Gallagher et al.*, 1998; *Ehlers and Farley*, 2003; *Reiners and Brandon*, 2006]. In this study, AFT and AHe thermochronology have been applied on basement, cover and magmatic rocks from the Apuseni Mountains to derive quantitative constraints on its exhumation history. Thermochronological data have been integrated with new kinematic field data in order to derive the associated tectonic evolution.

2. The Apuseni Mountains—A Transitional Orogen Between the Carpathians and Dinarides

[5] The Apuseni Mountains form an internal mountain belt with respect to the present-day Carpathian and Dinaridic-Hellenic belts and are situated at the transition between the Tisza, East Vardar and Dacia tectonic units (Figure 1). The East Vardar Ocean was probably obducted onto parts of Dacia during Late Jurassic times [*Schmid et al.*, 2008], followed by late Early Cretaceous ("Austrian" in local Romanian literature) obduction and continental collision between the Tisza and Dacia continental blocks [*Săndulescu*, 1988; *Csontos and Vörös*, 2004]. The latter is responsible for the eastward emplacement of a large sheet of East Vardar ophiolites (or Transylvanides) over the Dacia basement, which are recognized as far east as the East Carpathians [e.g., *Săndulescu and Visarion*, 1978; *Ionescu et al.*, 2009] (Figure 1). In the Apuseni Mountains, this was followed by intra-Turonian ("Mediterranean") westward back-vergent thrusting, creating the retro-vergent side of the orogen in a series of four main nappe units (Mecsek, Bihor, Codru and Biharia [e.g., *Săndulescu*, 1984; *Balintoni*, 1994; *Haas and Pero*, 2004; *Schmid et al.*, 2008, and references therein]; Figure 1).

2.1. Late Cretaceous Tectonics and Magmatism

[6] The Apuseni Mountains and the neighboring Transylvanian Basin experienced Late Cretaceous (late Turonian–early Campanian) extension [e.g., *Balintoni*, 1994]. In large areas, gradual subsidence and deepening of sedimentary facies is recorded by the post-collisional covers of "Gosau" type (part of the Remeți and Bozes flysches, Figure 2), associated with the contemporaneous formation of small grabens [*Balintoni*, 1994; *Willingshofer et al.*, 1999; *Schuller*, 2004]. Compression, recognized at the scale of the entire Romanian Carpathians, resumed during the late Senonian (late Campanian–Maastrichtian) "Laramian" phase [e.g., *Săndulescu*, 1984; *Balintoni*, 1994; *Schmid et al.*, 2008, and references therein]. Deformation generated structures which change strike from low-angle E-W trending nappe contacts with top-N vergence in the Southern Apuseni Mountains to N-S high-angle reverse faults with large along-strike offset components at the eastern margin of the Apuseni Mountains (Figures 1b and 1c) [see also *Bleahu et al.*, 1981; *Balintoni*, 1994]. The latest Cretaceous–earliest Paleogene post-collisional sedimentation spans several sequences of mainly continental terrigenous sedimentation [e.g., *Paraschiv*, 1979; *Bleahu et al.*, 1981].

[7] Deformation was coeval with and followed by latest Cretaceous intrusive and extrusive (sub-)volcanic Banatitic magmatism, recognized in a ~1500 km long curved belt stretching from the Apuseni Mountains to the central Balkans [e.g., *Berza et al.*, 1998; *Zimmerman et al.*, 2008]. Re-Os ages of Banatitic magmatic activity range between 88–81 Ma for the South Carpathians to 84–72 Ma for the Apuseni-Banat area [*Zimmerman et al.*, 2008]. For the Apuseni Mountains, K-Ar and $^{40}Ar/^{39}Ar$ ages indicate latest Cretaceous–Eocene cooling of the Banatites [*Bleahu et al.*, 1981; *Wiesinger et al.*, 2005]. Based on $^{40}Ar/^{39}Ar$ amphibole and biotite ages ranging between 89 Ma in the South Carpathians to 61 Ma in the Apuseni Mountains, *Wiesinger et al.* [2005] suggested three consecutive magmatic events: Turonian–Santonian, Campanian and Maastrichtian. The bulk of the Paleocene–Eocene ages are derived from older K-Ar measurements [*Bleahu et al.*, 1981] and represent cooling ages. The magmatic rocks are mostly extrusive (sub-) volcanic in the southern part of the Apuseni Mountains [*Seghedi*, 2004] and mostly intrusive in the northern part, except for part of the Vlădeasa volcano-plutonic complex (Figure 1c) [*Bleahu et al.*, 1981].

2.2. Post-Cretaceous Evolution of the Apuseni Mountains and Transylvanian Basin

[8] The post-Cretaceous tectonic evolution of the Apuseni Mountains is less well constrained. It is generally assumed that

Figure 1. (a) Tectonic map of the Eastern Alps-Carpathians-Dinarides-Balkans region (simplified after work by *Schmid et al.* [2008]) and its location in the topographic map of Europe (inset map in top left corner). Solid black line indicates the location of the cross-section and solid box indicates the location of the Apuseni Mountains. White lines indicate the outlines of the Pannonian and Transylvanian Basins and dashed black line indicates the border of Romania. BDVF is Bogdan-Voda Dragos-Voda fault. (b) Conceptual cross-section through the Apuseni Mountains, Transylvanian Basin and SE Carpathians (simplified after work by *Schmid et al.* [2008]). (c) Tectonic map of the Apuseni Mountains (modified after work by *Balintoni* [1994]). Solid black lines show the locations of cross-sections in Figure 12.

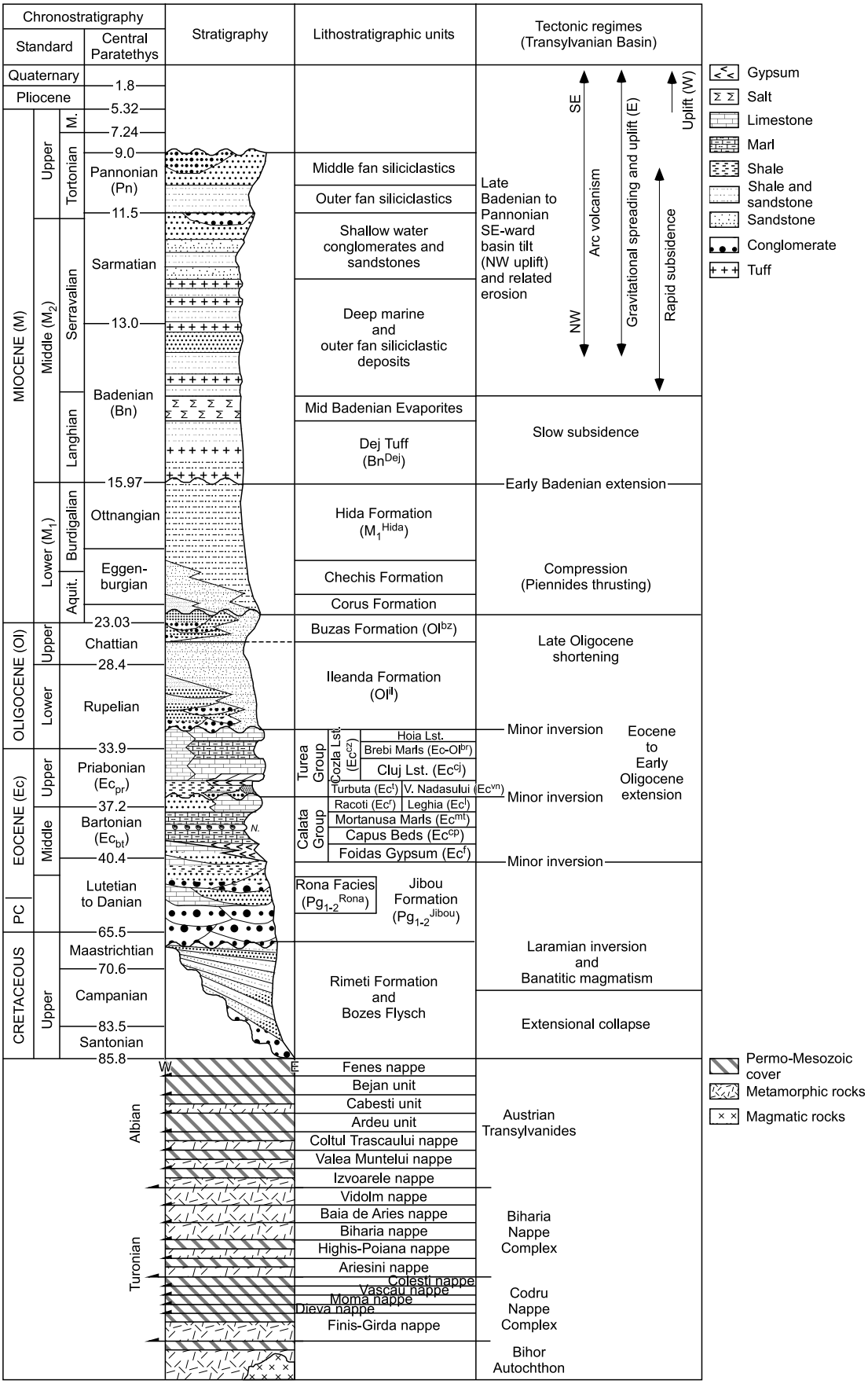
Chronostratigraphy
Standard
Central Paratethys
Stratigraphy
Lithostratigraphic units
Tectonic regimes (Transylvanian Basin)
Quaternary
Pliocene
1.8
5.32
MIOCENE (M)
Upper
M.
7.24
Tortonian
9.0
Pannonian (Pn)
11.5
Middle (M2)
Serravalian
Sarmatian
13.0
Badenian (Bn)
Langhian
Lower (M1)
Burdigalian
Ottnangian
15.97
Aquit.
Eggen-burgian
23.03
OLIGOCENE (Ol)
Upper
Chattian
28.4
Lower
Rupelian
33.9
EOCENE (Ec)
Upper
Priabonian (Ecpr)
37.2
Middle
Bartonian (Ecbt)
40.4
PC
Lutetian to Danian
65.5
CRETACEOUS
Upper
Maastrichtian
70.6
Campanian
83.5
Santonian
85.8
Middle fan siliciclastics
Outer fan siliciclastics
Shallow water conglomerates and sandstones
Deep marine and outer fan siliciclastic deposits
Mid Badenian Evaporites
Dej Tuff (Bn Dej)
Hida Formation (M1 Hida)
Chechis Formation
Corus Formation
Buzas Formation (Ol bz)
Ileanda Formation (Ol il)
Turea Group
Cozla Lst. (Ec cz)
Hoia Lst.
Brebi Marls (Ec-Ol br)
Cluj Lst. (Ec cj)
Turbuta (Ec t)
V. Nadasului (Ec vn)
Racoti (Ec r)
Leghia (Ec l)
Calata Group
Mortanusa Marls (Ec mt)
Capus Beds (Ec cp)
Foidas Gypsum (Ec f)
Rona Facies (Pg1-2 Rona)
Jibou Formation (Pg1-2 Jibou)
Rimeti Formation and Bozes Flysch
Late Badenian to Pannonian SE-ward basin tilt (NW uplift) and related erosion
SE
NW
Arc volcanism
Gravitational spreading and uplift (E)
Uplift (W)
Rapid subsidence
Slow subsidence
Early Badenian extension
Compression (Piennides thrusting)
Late Oligocene shortening
Minor inversion
Eocene to Early Oligocene extension
Minor inversion
Minor inversion
Laramian inversion and Banatitic magmatism
Extensional collapse
W.
E.
Albian
Turonian
Fenes nappe
Bejan unit
Cabesti unit
Ardeu unit
Coltul Trascaului nappe
Valea Muntelui nappe
Izvoarele nappe
Vidolm nappe
Baia de Aries nappe
Biharia nappe
Highis-Poiana nappe
Ariesini nappe
Colesti nappe
Vascau nappe
Moma nappe
Dieva nappe
Finis-Girda nappe
Austrian Transylvanides
Biharia Nappe Complex
Codru Nappe Complex
Bihor Autochthon
Gypsum
Salt
Limestone
Marl
Shale
Shale and sandstone
Sandstone
Conglomerate
Tuff
Permo-Mesozoic cover
Metamorphic rocks
Magmatic rocks

Figure 2

this area was part of the Paleogene–Miocene clockwise rotation and subsequent translation of the Tisza-Dacia block around the Moesian promontory [e.g., *Balla*, 1987; *Ratschbacher et al.*, 1993; *Pătraşcu et al.*, 1994; *Márton et al.*, 2007]. The kinematic effects in the area of the Apuseni Mountains are largely unknown. The only coherent deformation structures described to date are N-S striking faults at the eastern margin of the Apuseni Mountains, truncating Eocene sediments sealed by Oligocene cover units [i.e., the Puini thrust and its S-ward prolongation, *Schmid et al.*, 2008] (Figures 1b and 1c). Normal faulting led to the opening of NW-SE oriented middle Miocene basins at the western margin of the Apuseni Mountains (Figures 1b and 1c), which are filled with middle–upper Miocene shallow marine to lacustrine sediments [*Bleahu et al.*, 1981; *Balintoni and Vlad*, 1998; *Csontos et al.*, 2002]. Genetically related volcanism took place during the late Badenian–Pannonian (15–7 Ma), reaching its climax during the Sarmatian (K-Ar ages of 13.5 –10 Ma) [e.g., *Săndulescu et al.*, 1978; *Pécskay et al.*, 1995; *Roşu et al.*, 1997, 2004].

[9] In the Transylvanian Basin, Paleogene sediments crop out in the NW and consist of four transgressive-regressive cycles of continental deposits grading into shallow and deeper marine deposits separated by unconformities (Figure 2) [*Popescu*, 1984; *Hosu*, 1999]. Among these cycles, the first Paleocene–early Priabonian one starts with red continental and lacustrine sediments (Jibou Fm., Figure 2), and is a result of post-collisional erosional breakdown of the Cretaceous orogen [*Popescu*, 1984; *Krézsek and Bally*, 2006]. Outside the NW part of Transylvania, large parts of the basin indicate a widespread unconformity during Paleogene–lower Miocene times [e.g., *Paraschiv*, 1979]. Following minor early middle Miocene clastic/limestone deposition topped by thick tuffs (Dej) and regional salt deposition, the Transylvanian Basin records accelerated subsidence coeval with the deposition of up to 4 km of middle–upper Miocene sediments [*Krézsek and Bally*, 2006] (Figure 2). Notably, these are not associated with large-scale normal faulting and massive lithosphere attenuation, such as is the case in the Pannonian Basin [*Horváth et al.*, 2006; *Krézsek et al.*, 2010]. Toward the end of the Miocene, the external Carpathian collision resulted in compressional pulses in the Transylvanian Basin, which was subsequently exhumed and exposed to sub-aerial conditions at ~9 Ma [*Matenco et al.*, 2010].

3. Low-Temperature Thermochronology of the Apuseni Mountains

[10] To reconstruct the cooling and exhumation history of the Apuseni Mountains, samples were analyzed by low-temperature thermochronology (Figure 3 and Table 1). Sixteen new samples were analyzed by AFT; six of these were also analyzed by AHe (Table 1; "RO" samples). Four samples previously dated by AFT [*Sanders*, 1998] were reassessed using AHe dating (Table 1; "Carp" samples). See appendices A and B for a description of AFT and AHe analytical methods and data.

[11] The new AFT and AHe results were integrated with data from previously published fission track studies [*Sanders*, 1998; *Schuller*, 2004; *Schuller et al.*, 2009] (Table 1 and Figure 3). To allow distinguishing the timing of exhumation events in relation to the tectonic evolution of the Apuseni Mountains, samples are generically grouped in 5 formation age units based on structural inheritance and/or formation age: (1) Precambrian–Paleozoic crystalline basement together with its Permo-Mesozoic cover, (2) Upper Cretaceous Banatites, (3) Neogene volcanics, (4) Senonian and (5) Neogene sedimentary covers (Figure 3 and Table 1). The new AFT and AHe ages obtained in this study are from units 1, 2 and 3 only. Samples from Unit 1 are subsequently discussed as function of their position in tectonic units that were involved in the main late Early Cretaceous and Turonian collisional events (Bihor, Codru and Biharia nappes). Samples from the second and fourth unit were emplaced/deposited coeval with the "Laramian" tectonic events. Samples from the third and fifth unit were emplaced/deposited simultaneously with the rotation of Tisza-Dacia around the Moesian promontory and the East Carpathian collision. Note that, in the overall structure of the Apuseni Mountains, the geographical location of the Bihor Dome as an elevated region situated in the core of the Apuseni Mountains is discussed differently from the tectonic Bihor Nappe (Figure 3).

3.1. Discussion of Apatite Fission Track and (U-Th)/He Data

3.1.1. Precambrian–Paleozoic Crystalline Basement With Its Permo–Mesozoic Cover

[12] For Unit 1, new AFT central ages range between 82 ± 9 Ma and 25 ± 3 Ma ("RO" samples; Table 1 and Figures 3 and 4). Most basement samples pass the Chi-square test ($P(\chi^2) \geq 5\%$) [*Galbraith*, 1981], except for RO-16 and RO-23 (Table 1 and Figure 4). For some samples it was not possible to obtain sufficient track lengths to allow for a significant geological interpretation of the data (e.g., RO-25; Figure 4). However, on the overall, length data for basement samples show unimodal slightly negatively skewed track length distributions with mean track lengths (MTLs) ranging between 13.2 ± 2.4 μm and 14.2 ± 1.1 μm ("RO" samples; Table 1 and Figures 3 and 4). These are indicative for rapid cooling of basement samples through the APAZ with minor thermal disturbance afterwards. Etch pit diameters (D_{par}) for the basement samples range between 1.2 ± 0.2 μm and 1.7 ± 0.3 μm (Table 1), indicating fairly similar chemical compositions and relatively fluorine rich apatites [*Burtner et al.*, 1994] with a low resistance to annealing [e.g., *Ketcham et al.*, 1999]. Except for RO-34 (25 ± 3 Ma), AFT ages are similar to those reported by *Sanders* [1998] and *Schuller* [2004] (77 ± 4 Ma to 40 ± 3 Ma; Table 1 and Figure 3). The shorter overall MTLs of 13.6 ± 1.2 μm to 10.3 ± 2.3 μm reported by *Sanders* [1998] might be partially explained by the fact that *Sanders* [1998] did not normalize for track angle using the c-axis projection model of *Donelick et al.* [1999].

Figure 2. Simplified tectonostratigraphy of the NW Transylvanian Basin [*Krézsek and Bally*, 2006] and tectonostratigraphic positions of nappe complexes of the Mesozoic tectonic units [*Schuller*, 2004]. Paleogene formation names are based on *Popescu* [1984], *Proust and Hosu* [1996], *Hosu* [1999], and *Krézsek and Bally* [2006]. Standard absolute ages are from *Gradstein and Ogg* [2004]. Paratethys stage boundaries follow *Rögl* [1996], *Filipescu* [2001], and *Krézsek and Filipescu* [2005].

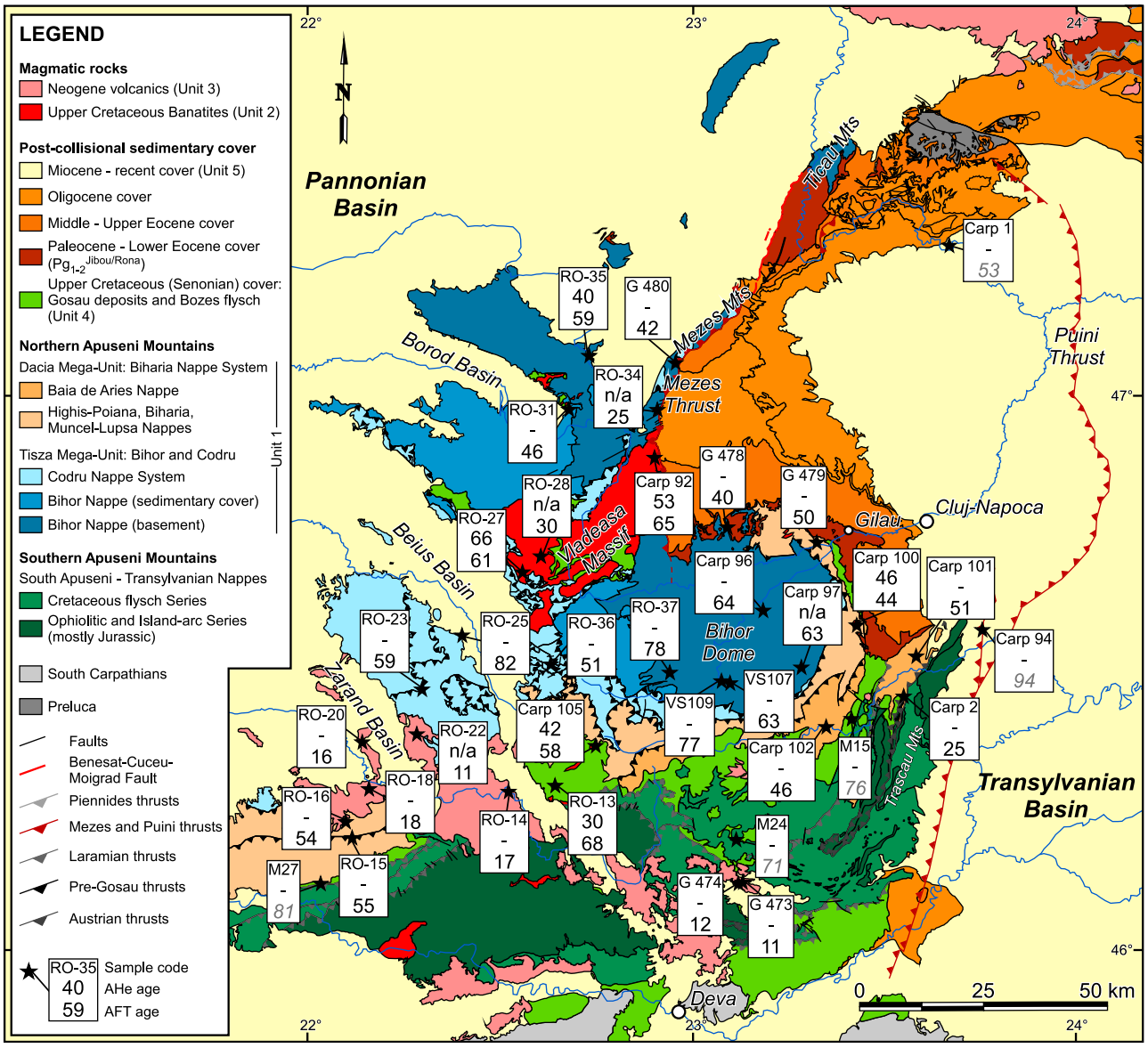

Figure 3. Tectonic map of the Apuseni Mountains (modified after *Balintoni* [1994]) depicting new and previously published low-temperature thermochronological ages. Stars show sample locations and numbers in boxes from top to bottom represent sample code, AHe age and AFT age, respectively. "RO" sample codes are from this study, "Carp/G" sample codes are AFT data of *Sanders* [1998] and "VS/M" sample codes are AFT data of *Schuller* [2004]. AFT ages are central ages [*Galbraith and Laslett*, 1993] (see Tables 1 and A1). Depicted AHe ages are the error weighted averages of the α-corrected single grain ages (see Tables 1, B1 and B2). Samples with AHe ages marked as "n/a" represent samples for which average AHe age could not be calculated (see text for further details). Ages in gray italics represent non-reset ages.

[13] AHe dating yields an age of 40 ± 14 Ma for basement sample RO-35 (Table 1 and Figure 3). ^{4}He and ^{232}Th quantities for sample RO-34 were outside detection limits (Table B1), and thus AHe single crystal ages have not been taken into account for further interpretation (see appendix B for further details). Sample Carp 97 yields an AHe age (124 ± 11 Ma; Table B2) much older than its corresponding AFT age (63 ± 5 Ma; Table 1). During selection of apatite crystals it was noted that many apatites from this sample contain small fluid inclusions. The presence of undetected micro-inclusions could be the cause for the erroneously old AHe ages for this sample [e.g., *Lippolt et al.*, 1994; *Farley*, 2002]. AHe results from this sample were omitted from further geological interpretations.

[14] Figure 5 shows the relation between AFT age versus sampling elevation and MTL for basement samples from the Apuseni Mountains (Unit 1), subdivided into the Bihor, Codru and Biharia nappes. Samples RO-37, Carp 96, Carp 97, VS107 and VS109 are all from the same tectonic block of the Bihor Dome (Figure 3; Bihor Nappe). Of these five samples, the sample at the highest elevation (Carp 97, MTL of 12.9 ± 1.7 μm) is slightly more annealed than the samples

Table 1. Overview Sample Details and Thermochronological Data

Sample Details[a]					AFT Results[b]							AHe Results[c]		
Sample Code	Tectonic Unit	Lithology	Geologic Time	Elevation (m)	$N_{Gr.}$	$P(\chi^2)$ (%)	Disp. (%)	Age ± 1σ (Ma)	MTL ± SD_L (μm)	N_L	D_{par} ± SD_{Dpar} (μm)	Age ± 1σ (Ma)	$N_{Repl.}$	$N_{Av.}$
Unit 1: Precambrian–Paleozoic Crystalline Basement and Permo-Mesozoic Cover														
RO-15	Biharia	Quartzite	Paleozoic	369	21	5	45	55 ± 11	13.4 ± 1.3	38	1.4 ± 0.2	-	-	-
RO-16	Biharia	Metapelite	Paleozoic	282	7	<5	18	54 ± 7	14.2 ± 1.1	33	1.3 ± 0.1	-	-	-
RO-23	Codru	Sandstone	Ne-Jur. sup.	358	22	<5	27	59 ± 8	13.6 ± 1.3	44	1.7 ± 0.3	-	-	-
RO-25	Codru	Quartzite	Permian	296	15	95	0	82 ± 9	13.2 ± 2.4	7	1.6 ± 0.3	-	-	-
RO-34	Bihor	Micaschist	Middle Prec.	562	38	82	2	25 ± 3	14.1 ± 1.5	66	1.4 ± 0.3	n/a	3	0
RO-35	Bihor	Micaschist	Precambrian	338	34	22	14	59 ± 7	14.2 ± 0.9	130	1.5 ± 0.1	40 ± 14	4	1
RO-36	Codru	Granite	Hercynian	1165	5	62	0	51 ± 17	-	-	1.2 ± 0.2	-	-	-
RO-37	Bihor	Micaschist	Paleozoic	756	8	93	0	78 ± 22	13.4 ± 1.5	26	1.3 ± 0.3	-	-	-
Carp 96	Bihor	Schist	-	1000	36	-	17	64 ± 7	13.6 ± 1.2	38	-	-	-	-
Carp 97	Bihor	Granite	Variscan	1730	33	-	27	63 ± 5	12.9 ± 1.7	87	-	n/a	3	0
Carp 101	Biharia	Schist	-	450	30	-	13	51 ± 4	12.8 ± 1.5	100	-	-	-	-
Carp 102	Biharia	Gneiss	-	550	26	-	12	46 ± 4	13.3 ± 1.5	100	-	-	-	-
G 478	Bihor	Granite	Variscan	600	15	-	12	40 ± 3	10.3 ± 2.3	100	-	-	-	-
G 480	Bihor	Gneiss	-	600	20	-	78	42 ± 12	-	-	-	-	-	-
VS107	Bihor	Granite	Variscan	1500	20	65	-	63 ± 4	13.5 ± 1.1	n/a	-	-	-	-
VS109	Bihor	Micaschist	Variscan	1500	20	20	-	77 ± 4	-	-	-	-	-	-
Unit 2: Upper Cretaceous Banatites														
RO-13	Luncsoara M.	Diorite	Senonian	378	21	98	0	68 ± 9	15.1 ± 0.9	108	2.1 ± 0.3	30 ± 6	4	2
RO-27	Budureasa M.	Granodiorite	Senonian	685	34	57	7	61 ± 7	14.7 ± 1.0	90	1.7 ± 0.2	66 ± 7	4	4
RO-28	Vladeasa M.	Rhyolite	Senonian	921	28	12	23	30 ± 4	14.6 ± 1.0	46	1.7 ± 0.4	n/a	3	0
RO-31	Borod M.	Rhyolite	Senonian	459	34	<5	27	46 ± 6	13.9 ± 1.5	14	2.1 ± 0.2	-	-	-
Carp 92	-	Dacite	Senonian	600	34	-	14	65 ± 5	14.2 ± 1.3	106	-	53 ± 3	3	3
Carp 100	-	Andesite	Senonian	580	43	-	12	44 ± 3	12.9 ± 1.7	100	-	46 ± 3	3	3
Carp 105	-	Granite	Senonian	350	14	-	14	58 ± 6	12.9 ± 0.9	24	-	42 ± 2	3	3
G 479	-	Andesite	Senonian	500	23	-	5	50 ± 5	12.3 ± 2.2	26	-	-	-	-
Unit 3: Neogene Volcanics														
RO-14	-	Andesite	Neogene	238	14	100	0	17 ± 4	14.7 ± 0.8	15	2.3 ± 0.3	--	-	-
RO-18	-	Andesite	Neogene	200	10	86	0	18 ± 6	12.2 ± 1.9	4	1.7 ± 0.1	--	-	-
RO-20	-	Andesite	Neogene	182	4	97	0	16 ± 9	14.7 ± 1.6	16	2.3 ± 0.4	--	-	-
RO-22	-	Andesite	Neogene	307	27	72	1	11 ± 2	15.2 ± 0.9	25	2.2 ± 0.4	n/a	3	0
G 473	-	Andesite	Neogene	600	20	-	14	11 ± 1	14.2 ± 1.3	7	-	-	-	-
G 474	-	Andesite	Sarmatian	600	19	-	10	12 ± 2	-	-	-	-	-	-
Unit 4: Senonian Sedimentary Cover														
Carp 2	Gosau	Sandstone	Senonian	500	20	-	83	25 ± 6	12.9 ± 1.4	50	-	-	-	-
M24	Upper Gosau	Sandstone	Maastrichtian	-	20	57	-	*71 ± 4*	-	-	-	-	-	-
M27	Upper Gosau	Sandstone	Maastrichtian	-	20	57	-	*81 ± 4*	-	-	-	-	-	-
M15	Upper Gosau	Sandstone	Campanian	-	20	59	-	*76 ± 4*	-	-	-	-	-	-
Unit 5: Neogene Sedimentary Cover														
Carp 1	-	Sandstone	Oligo-Miocene	450	20	-	16	*53 ± 7*	11.9 ± 1.4	45	-	-	-	-
Carp 94	-	Sandstone	Badenian	500	49	-	39	*94 ± 9*	-	-	-	-	-	-

[a]Sample codes "RO" are samples from this study. "Carp"/"G" sample codes are AFT samples from the study of *Sanders* [1998], of which some were reassessed by AHe in this study. "VS"/"M" sample codes are from the study of *Schuller* [2004] and *Schuller et al.* [2009].

[b]$N_{Gr.}$ is number of dated apatite crystals; $P(\chi^2)$ is χ^2 probability [*Galbraith*, 1981]; Disp. is dispersion in single grain ages [*Galbraith and Laslett*, 1993]; Age is central age [*Galbraith and Laslett*, 1993]; Ages in italics represent non-reset ages; MTL ± SD_L is mean track length ± standard deviation of the confined track length distribution. Confined track lengths for samples from this study ("RO" codes) are normalized for track angle using the c-axis projection model of *Donelick et al.* [1999]; N_L is number of horizontal confined tracks; D_{par} ± SD_{Dpar} is average etch pit diameter ± standard deviation [*Donelick*, 1993]. This table only reports D_{par} values measured on grain mounts, but D_{pars} were determined for both grain and length mounts and overlap within error (Table A1). See Appendix A for details on AFT analytical methods and data.

[c]Age is error weighted average of replicate AHe single crystal ages ± 1σ standard error (see Tables B1 and B2). Note that this error weighted average age has been used for further interpretation. Samples marked with n/a represent samples for which average could not be calculated due to high blank/sample ratios, high dispersions in single crystal ages and/or samples for which $Age_{AHe} \gg Age_{AFT}$. These samples have not been taken into account for further interpretation; $N_{Repl.}$ is number of replicate single crystal measurements; $N_{Av.}$ is number of single crystal ages taken into account for calculation of error weighted average age. See Appendix B for details on AHe analytical methods and data.

at lower elevations (e.g., RO-37, MTL of 13.4 ± 1.5 μm), but the sample at the lowest elevation seems to have the oldest age (RO-37, 78 ± 22 Ma). The maximum horizontal distance between these samples is ~30 km (Figure 3), which is too large to derive a proper age-elevation relationship. The data do, however, suggest that AFT cooling ages in the Bihor Dome are, within uncertainty, indistinguishable over a ~1000 m vertical sample interval (Figure 5; 78 ± 22 Ma to 63 ± 5 Ma). This observation limits the interpretation of rapid cooling of the Bihor Dome to the latest Cretaceous time interval. AFT ages from samples of the Bihor (RO-35) and Codru nappes (RO-25 and RO-23) located further away from the Bihor Dome, overlap this age range within error (Figure 5 and Table 1). Samples from the Biharia nappe have younger AFT ages ranging between 55 ± 11 Ma and 46 ± 4 Ma (Figure 5 and Table 1), suggesting early–middle

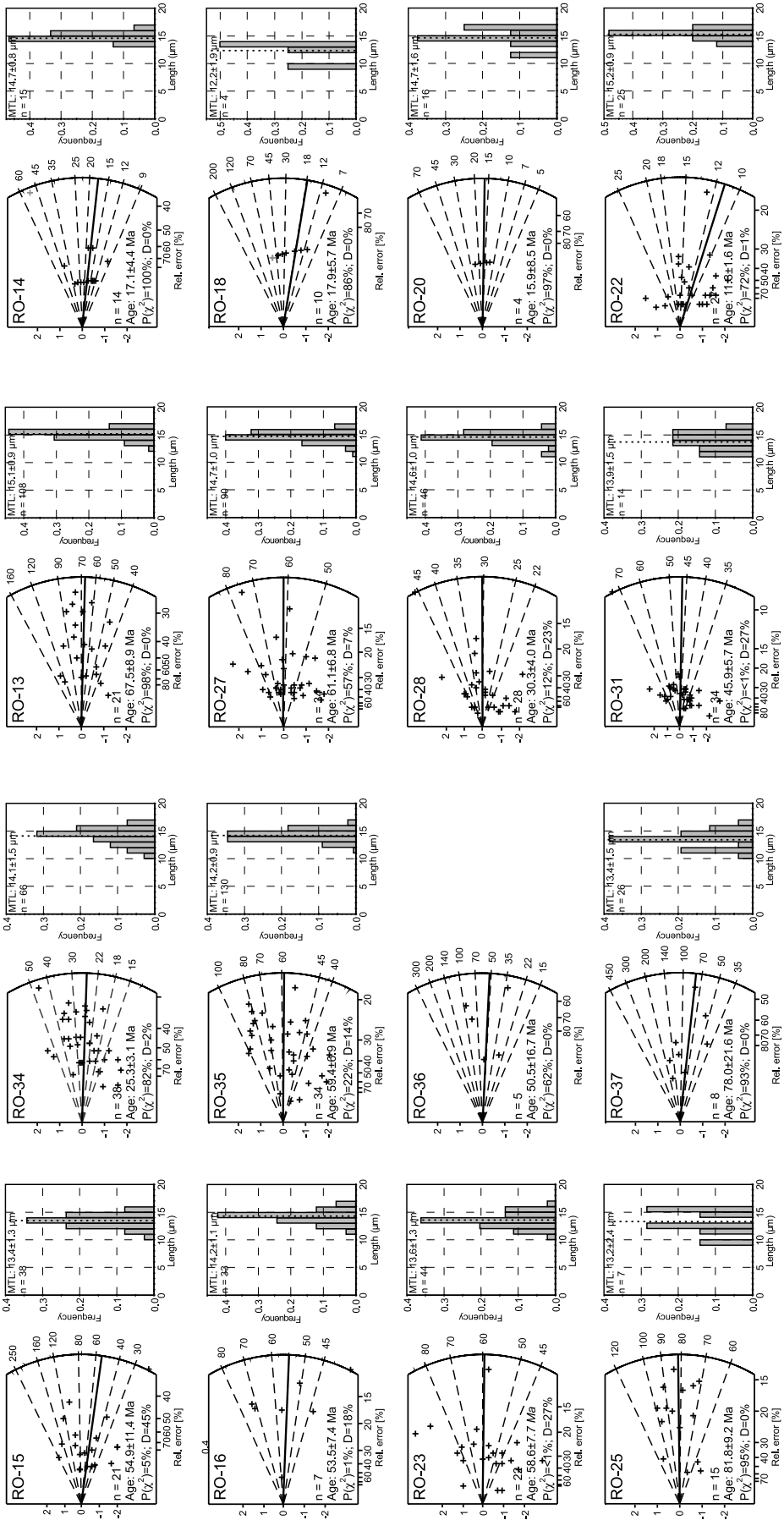

Figure 4. New AFT data for the Apuseni Mountains ("RO" samples; also see Table A1). The radial plots show AFT single grain ages (n is number of counted grains). Reported age and solid black line represent the central age. $P(\chi^2)$ is Chi-square (χ^2) probability. D is dispersion in single grain ages. For Neogene volcanic samples RO-14 and RO-18, AFT central ages were calculated without the rounded and inherited detrital grains (depicted in gray; see text for further explanation). The histograms show c-axis projected horizontal confined track length distributions. Reported MTL and dashed line are c-axis projected mean track length ± standard deviation. N is number of measured horizontal confined tracks.

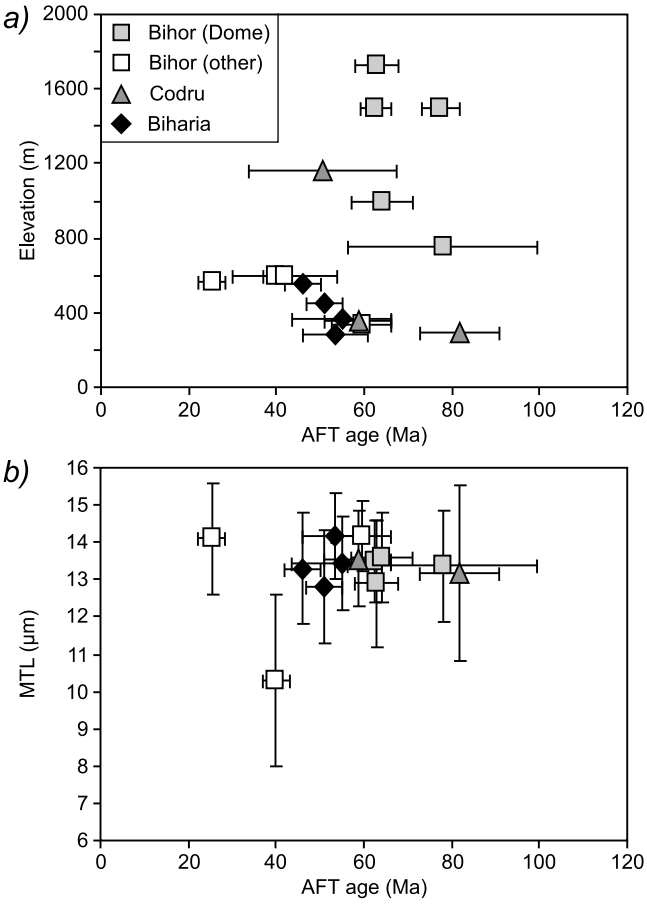

Figure 5. AFT age versus (a) sample elevation and (b) MTL for samples from the crystalline basement and cover units (Unit 1). Samples are further subdivided based on tectonic unit (i.e., Bihor, Codru and Biharia nappes; Table 1). See text for further explanation.

Eocene cooling. Two Bihor nappe samples from the most northern margin of the Bihor Dome (near the contact with the Transylvanian Basin) record similar younger AFT ages of 40 ± 3 Ma and 42 ± 12 Ma (G 478 and G 480). One Bihor nappe sample from the Mezeş Mountains records the youngest AFT age of 25 ± 3 Ma (RO-34; Figures 3 and 5 and Table 1).

3.1.2. Upper Cretaceous Banatites

[15] Upper Cretaceous Banatite samples of Unit 2 yield AFT ages ranging between 68 ± 9 and 30 ± 4 Ma ("RO" samples; Table 1 and Figures 3 and 4). Three out of four Banatite samples pass the Chi-square test and have narrow unimodal track-length distributions with MTLs ranging between 15.1 ± 0.9 μm and 14.6 ± 1.0 μm (Table 1 and Figure 4), indicative for rapid cooling through the APAZ. Sample RO-31 fails the Chi-square test and has a track-length distribution with a MTL of 13.9 ± 1.5 μm (Table 1 and Figure 4). The number of length measurements for this sample is however insufficient to allow for a clear interpretation of the data. Mean D_{par} values of 1.7 ± 0.4 μm to 2.1 ± 0.3 μm obtained for the Banatite samples (Table 1) are indicative of little chemical variation and fairly low resistance to annealing [*Burtner et al.*, 1994; *Ketcham et al.*, 1999]. The new AFT ages are in agreement with previously published AFT data, which show a similar AFT age range between 65 ± 5 Ma and 44 ± 3 (Table 1 and Figure 3) [*Sanders*, 1998].

[16] AHe dating yields an age of 66 ± 7 Ma for RO-27, overlapping its AFT age within error (Table 1 and Figure 3). Younger AHe ages of 53 ± 3 to 30 ± 6 Ma were obtained for the other Banatite samples (Table 1 and Figure 3). Sample RO-28 yields very disperse AHe single crystal ages (105 ± 28, 158 ± 22 and 70 ± 30 Ma, Table B1), much older than its AFT age. Apatite crystals from this sample have low U-contents (<5 ppm) and might thus be sensitive to potential ^{4}He implantation from surrounding U-Th rich rock components [e.g., *Spiegel et al.*, 2009], resulting in too old AHe ages. AHe ages of this sample have been omitted from further geological interpretations.

[17] AFT ages of four samples (68 ± 9–58 ± 6 Ma; Table 1) and one AHe age (66 ± 7 Ma) are indistinguishable within errors from ^{40}Ar/^{39}Ar amphibole and biotite ages (~61–72 Ma) [*Wiesinger et al.*, 2005], suggesting that they record rapid latest Cretaceous magmatic cooling of intrusive rocks to shallow depths. The younger AFT (50 ± 5–30 ± 4 Ma) and AHe ages (53 ± 3–30 ± 6 Ma; Table 1) for the other samples suggest that these samples recorded a cooling event post-dating magmatic emplacement.

3.1.3. Neogene Volcanics

[18] Neogene volcanics (andesites) of Unit 3 yield AFT ages ranging between 11 ± 2 Ma and 18 ± 6 Ma (Table 1 and Figures 3 and 4). The AFT ages compare well with previously published AFT ages (11–15 Ma) [*Sanders*, 1998] and are indistinguishable within errors from K-Ar ages of 15–7 Ma [*Pécskay et al.*, 1995; *Roşu et al.*, 1997]. Samples RO-14 and RO-18 contain some rounded apatite crystals with AFT single grain ages of ~45–60 Ma (not taken into account for calculation of AFT ages; Figure 4). These few single grain ages are indistinguishable from the AFT ages obtained for the surrounding host rocks (Figure 3), suggesting a minor detrital influx for these two samples. Samples have long MTLs of 14.7 ± 1.6 μm to 15.2 ± 0.9 μm (Table 1 and Figure 4) and 14.2 ± 1.3 μm [*Sanders*, 1998]. The narrow track length ranges with the majority of individual tracks between 13–17 μm (Figure 4) suggest rapid middle Miocene magmatic cooling without thermal disturbance afterwards. D_{par} values ranging between 1.7 ± 0.1 μm and 2.3 ± 0.4 μm (Table 1) are indicative of little chemical variation and fairly low resistance to annealing [*Burtner et al.*, 1994; *Ketcham et al.*, 1999].

[19] Sample RO-22 yields disperse AHe single grain ages (284 ± 34, 24 ± 7 and 47 ± 43 Ma; Table B1), much older than the AFT and extrusion ages. Inspection of the AFT mount of this sample indicated the presence of numerous small solid and fluid inclusions, which could play a role in the age dispersion and anomalously old AHe ages that were obtained for this sample [e.g., *Lippolt et al.*, 1994; *Farley*, 2002]. Furthermore, apatite grains from this sample have low U contents (<5 ppm) and might thus be sensitive to potential ^{4}He implantation from surrounding U-Th rich rock components [e.g., *Spiegel et al.*, 2009]. AHe ages of this sample have been omitted from further geological interpretations.

3.1.4. Senonian and Neogene Sedimentary Covers

[20] AFT data for the Senonian and Neogene sedimentary covers are available from *Sanders* [1998], *Schuller* [2004], and *Schuller et al.* [2009]. Their data show that only one

sample from the Senonian sedimentary cover (Unit 4) has been reset with respect to its stratigraphic age, with an AFT age of 25 ± 6 Ma (Carp 2; Table 1 and Figure 3) [*Sanders*, 1998]. The high dispersion in single grain ages (83%) and the relatively short MTL (12.9 ± 1.4 μm; Table 1) [*Sanders*, 1998] suggest considerable heterogeneity and prolonged residence in the APAZ. This sample comes from eastern margin of the Apuseni Mountains close to the Puini thrust. Three other Senonian samples dated for AFT by *Schuller* [2004] have homogeneous non-reset (i.e., provenance) AFT ages of 71 ± 4 Ma to 81 ± 4 Ma ("M" samples; Table 1 and Figure 3). These Campanian–Maastrichtian sediments did not experience a thermal overprint after sedimentation [*Schuller et al.*, 2009].

[21] Two Neogene sediment samples (Unit 5) dated for AFT by *Sanders* [1998] also lack a significant thermal overprint after sedimentation. This is suggested by homogeneous non-reset (provenance) ages of 53 ± 7 Ma and 94 ± 9 Ma (Carp 1 and Carp 94; Table 1 and Figure 3).

3.2. Thermal Modeling

[22] Time–temperature paths were modeled with the HeFTy program [*Ketcham*, 2005a], using both AFT age and length data and AHe single crystal ages integrated with geological constraints (Figure 6). Time-temperature histories for samples that were reassessed by AHe ("Carp" samples) were modeled using AHe data only, in combination with AFT age constraints of *Sanders* [1998].

[23] The best time-temperature constraints are available for the Banatites, with Re-Os ages, $^{40}Ar/^{39}Ar$ amphibole and biotite ages and AFT and AHe cooling ages. The Re-Os ages determine the crystallization age of the Banatites at 80.1–78.7 Ma [*Zimmerman et al.*, 2008]. Furthermore, $^{40}Ar/^{39}Ar$ amphibole and biotite dating, with closure temperatures of ~500°C and ~300°C, respectively [*Harrison*, 1981; *Harrison et al.*, 1985], indicates that the Banatites cooled below temperatures of ~300°C around 78–61 Ma [*Wiesinger et al.*, 2005]. Model results show that all Banatite samples rapidly cooled to temperatures <160°C around 75–65 Ma at ~50 ± 20°C/Ma (Figure 6a). This age range is interpreted to represent magmatic cooling. Sample RO-27 cooled to temperatures below ~40°C during the latest Cretaceous and shows no thermal overprint afterwards, whereas results for the other Banatite samples suggest younger cooling episodes post-dating magmatic emplacement (Figure 6a). Modeling results of three samples suggest early–middle Eocene (55–45 Ma) cooling from 120–80°C to surface temperatures at rates of 16 ± 7°C/Ma (Carp 105, Carp 100 and Carp 92; Figure 6a). Modeling results of the other two samples of Unit 2 suggest early Oligocene (35–25 Ma) cooling from 120–50°C to 45–15°C at rates of 9 ± 7°C/Ma (RO-13 and RO-28; Figure 6a). It is likely that the early–middle Eocene and the early Oligocene cooling episodes are of tectonic nature, since they take place long after termination of Banatite magmatism.

[24] For the crystalline basement, only two samples yield enough track length data to allow thermal modeling (Figure 6b). One model constraint is provided by zircon fission track ages of 95 to 85 Ma for the Bihor nappe [*Schuller*, 2004] (Figure 6b). Model results for sample RO-35 indicate rapid latest Cretaceous (70–62 Ma) cooling of 90 ± 57°C at a rate of 11 ± 7°C/Ma (including the error bar on the modeled good fit paths), slowing down to ~2.5°C/Ma in the Paleocene (Figure 6b). Although less well constrained due to the absence of AHe data, model results of RO-34 suggest an increase in cooling around 30–25 Ma (Figure 6b).

4. Paleogene Kinematics of the Apuseni Mountains in the Vicinity of the Transylvanian Basin

[25] The AFT and AHe data indicate Paleogene post-collisional exhumation events in the Northern Apuseni Mountains, potentially of tectonic nature. In order to link these events with the kinematic evolution, fieldwork was carried out in the areas where Paleogene sediments crop out in the proximity of the Apuseni Mountains. These areas stretch from Someş-Odorhei in the north to Turda in the south (Figure 7). Here, the NE part of the Apuseni Mountains is covered by Tertiary sediments of the Transylvanian Basin. The sediments of the Transylvanian Basin are in direct contact with Miocene sediments of the Pannonian Basin in a narrow area between the Mezeş Mountains and the basement "island" of the Ţicău Mountains (Figure 7). Paleogene sediments are generally eroded near the Apuseni Mountains and are gradually covered basin-wards beneath Miocene deposits. South of Cluj-Napoca, on the western flank of the Trascău Mountains, Paleogene–Miocene deposits nonconformably cover the Southern Apuseni nappe pile, while on the eastern flank Miocene deposits are in direct contact with these nappe units (Figure 7).

[26] Outcrop-scale structures, such as folds, conjugate fault sets and fault planes with kinematic indicators (e.g., slickensides, Riedels, shear-bands) [*Simpson and Schmid*, 1983; *Angelier*, 1994] were measured in the field (Figures 7–11). These new field data have been integrated with data from adjacent areas [e.g., *Ciulavu*, 1999; *Györfi et al.*, 1999; *Fodor et al.*, 1999] as well as data from geological maps, high-resolution field mapping studies [e.g., *Vlaicu-Tătărîm*, 1963; *Popescu*, 1984; *Proust and Hosu*, 1996; *Hosu*, 1999], which are correlated at depth with geological cross-sections [e.g., *Ştefănescu et al.*, 1988] and connected with seismic interpretations of the Transylvanian and Pannonian Basins [e.g., *Ciulavu et al.*, 2002; *Krézsek and Bally*, 2006]. Field mapping allowed the construction of kinematic cross-sections, illustrating the deformation style across major structures (Figure 8). Because most of the measurements were performed at or near map-scale deformation structures, the analysis of transport and kinematic directions was preferred over a paleostress analysis. Fault separation was performed mainly in the field by discriminating the relative timing between sets of structures. Deformation episodes were subsequently dated by correlation with associated syn-tectonic sedimentation and/or seismic analysis. For instance, the Upper Cretaceous Banatites are a good marker in order to discriminate Tertiary from Cretaceous structures.

[27] Overall, the data demonstrate that relevant post-collisional deformation is concentrated in rocks of Paleocene–Eocene age, while Oligocene–Miocene strata are generally sub-horizontal (e.g., Figure 8). Except for the contact zone between the Northern Apuseni Mountains and the Pannonian and Transylvanian Basins, the field area shows minor post-collisional deformation (Figure 7). A larger number of deformation structures are concentrated in three main areas, i.e., around the Mezeş Mountains and Vlădeasa Massif, the tran-

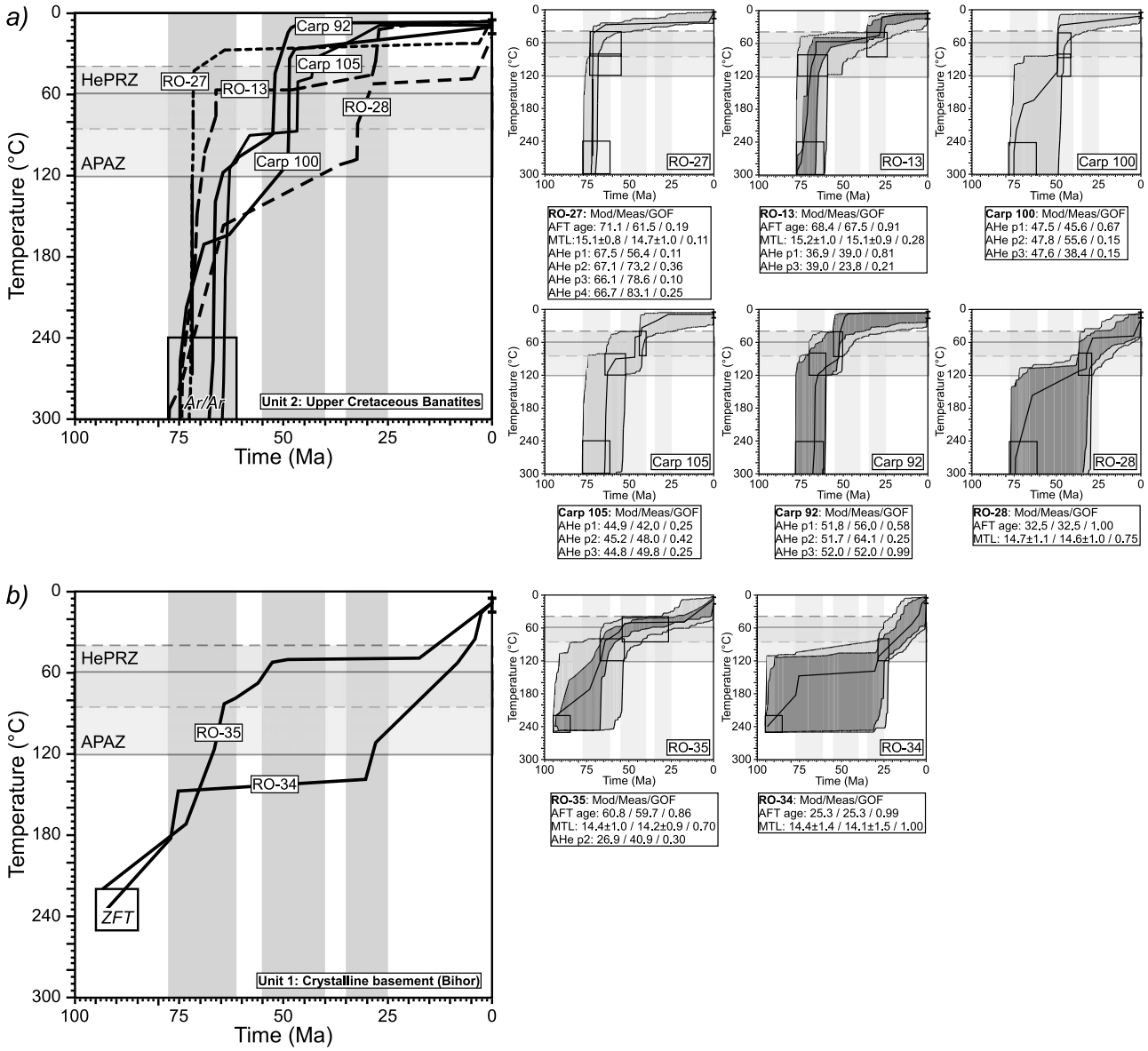

Figure 6. Thermal modeling results of AFT and AHe data (see appendices A and B for modeling parameters). The APAZ and HePRZ are shown in gray shades. Solid black boxes represent modeling constraints (see text for further explanation). Present-day surface T is set to 10 ± 5°C. To allow a good comparison of modeling results per unit, the best fit time-temperature paths are depicted in (left) the main graphs. The full modeled time-temperature histories including dark-gray and light-gray envelopes, encompassing statistically good-fits (GOF > 0.5) and acceptable fits (0.05 < GOF < 0.5), respectively (where GOF is the goodness of fit) [*Ketcham*, 2005a], are depicted in the (right) smaller graphs. Numbers in boxes represent sample codes. Text boxes show modeled (Mod.) against measured (Meas.) ages and MTLs and the GOF. Periods of increased modeled exhumation are highlighted in gray shades. (a) Upper Cretaceous Banatites (Unit 2). (b) Precambrian–Paleozoic crystalline basement and Permo–Mesozoic cover units (Unit 1).

sition between the Mezeş and Ţicău Mountains, and the area SW of Cluj Napoca (Figure 7).

4.1. The Mezeş Mountains and Vlădeasa Massif

[28] The most apparent map-scale structure in the study area is a NNE-SSW to N-S trending fault that limits the eastern margin of the Mezeş Mountains and Vlădeasa Massif (Figure 7), commonly referred to as the Mezeş Thrust (MT) [*Balintoni*, 1994]. Along this fault-contact, pre-Tertiary basement and Banatites are thrust eastward over Paleogene sediments of the Transylvanian Basin. The MT prolongation S-wards into the Bihor Dome is unknown (Figure 7).

[29] Field mapping indicates gradual tilting and deformation of strata in the MT footwall (Figures 8a–8g). Tilting at the fault contact varies from 10° (Figures 8b, 8c, and 8f)

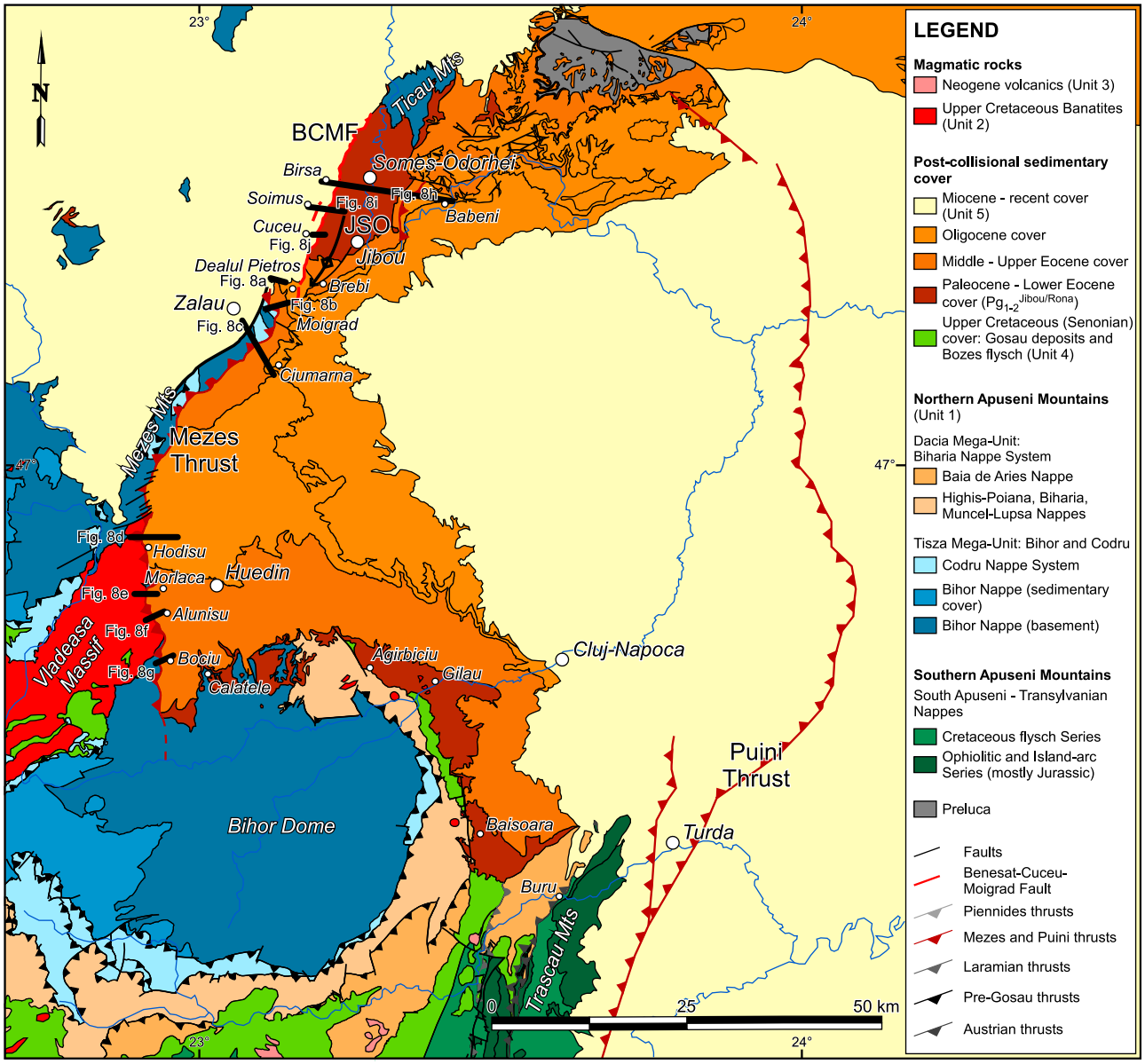

Figure 7. Structural map of the NE border of the Apuseni Mountains [after *Balintoni*, 1994] with locations of kinematic sections (solid black lines) of Figure 8.

to overturned strata (Figures 8a, 8d, 8e, and 8g), indicating E-W to ENE-WSW shortening directions (Figure 10a). Along the Dealul Pietros section (Figure 8a), the Paleocene–lowermost Oligocene strata are overturned in a km-size drag-fold, truncated by secondary thrusts that displace the Banatites in map-view [*Vlad et al.*, 1994]. This geometry requires a kilometers-scale thrust offset that has been subsequently eroded. This large-scale geometry is local; elsewhere the overturning of strata is localized near the MT. In other areas, drag-folding is partly accommodated by detachment folds in the soft clays below the Cluj Limestone, such as in the Morlaca profile (Figure 8e). Local tear faulting accommodates lateral variations in MT offset, such as at Bociu (Figures 8g and 9a).

Figure 8. Kinematic sections (see Figure 7 for locations) through the Mezeş Mountains and Vlădeasa Massif: (a) Dealul Pietros, (b) SW of Moigrad, (c) Ciumarna, (d) Hodişu, (e) Morlaca, (f) Alunişu, and (g) Bociu, and from the transition area between the Mezeş and Ţicău Mountains: (h) Birsa–Băbeni, (i) Şoimus, and (j) Cuceu. Sections (no vertical exaggeration) have been constructed based on field data and 1:50,000 and 1:200,000 geological maps of the Geological Institute of Romania [*Petrescu and Drăghici*, 1964; *Petrescu and Grigorescu*, 1974; *Petrescu et al.*, 1975; *Vlad and Romanoschi*, 1987; *Vlad et al.*, 1994]. See Figure 2 for an explanation of abbreviations used for lithostratigraphic units. Numbers in boxes represent measurement stations (see Figures 10 and 11 for locations). Note that the sections are more detailed than the large-scale structural map of Figure 7.

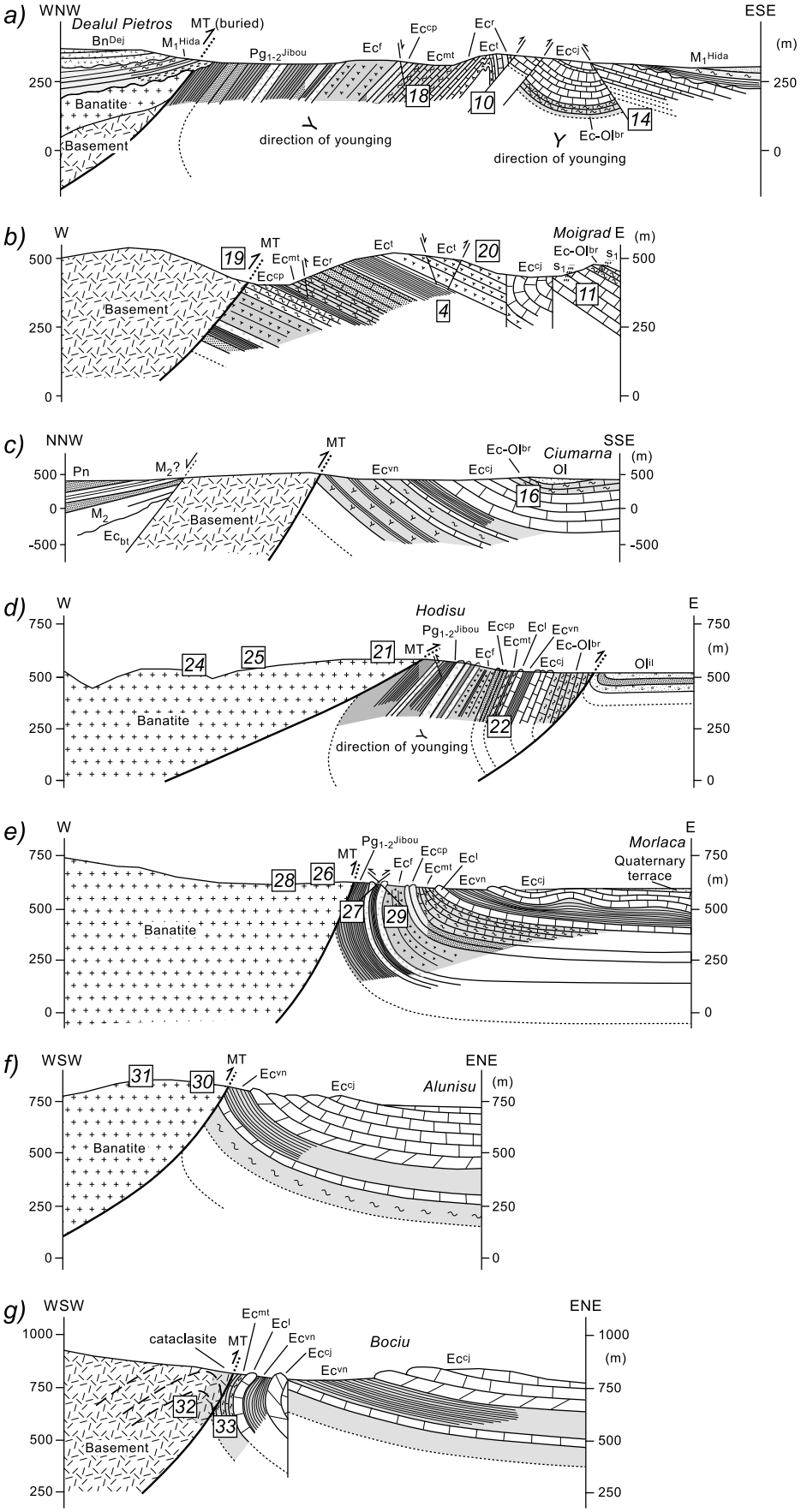
a)
WNW
ESE
Dealul Pietros
MT (buried)
BnDej
M1Hida
Pg1-2Jibou
Ecf
Ecmt
Ecp
Ecr
Ect
Ecj
M1Hida
(m)
250
0
Banatite
Basement
18
10
14
direction of younging
Ec-OlBr
direction of younging
b)
W
Moigrad
E
(m)
500
250
0
19
MT
Ecmt
Ecr
Ecp
Ect
Ect
20
Ecj
Ec-OlBr
s1
s1
11
4
Basement
c)
NNW
SSE
MT
Pn
M2?
Ecvn
Ecj
Ec-OlBr
Ciumarna
Ol
(m)
500
0
-500
16
M2
Ecbt
Basement
d)
W
E
Hodisu
750
500
250
0
(m)
Pg1-2Jibou
Ecp
Ecl
Ecvn
Ecmt
Ec-OlBr
Ecf
Ecj
Olil
24
25
21
MT
22
Banatite
direction of younging
e)
W
E
Morlaca
Quaternary
terrace
750
500
250
0
(m)
Pg1-2Jibou
MT
Ecf
Ecp
Ecmt
Ecl
Ecvn
Ecj
28
26
27
29
Banatite
f)
WSW
ENE
MT
Ecvn
Ecj
Alunisu
(m)
750
500
250
0
31
30
Banatite
g)
WSW
ENE
Ecmt
Ecl
cataclasite
MT
Ecvn
Ecj
Bociu
Ecj
Ecvn
1000
750
500
250
(m)
32
33
Basement

Figure 8

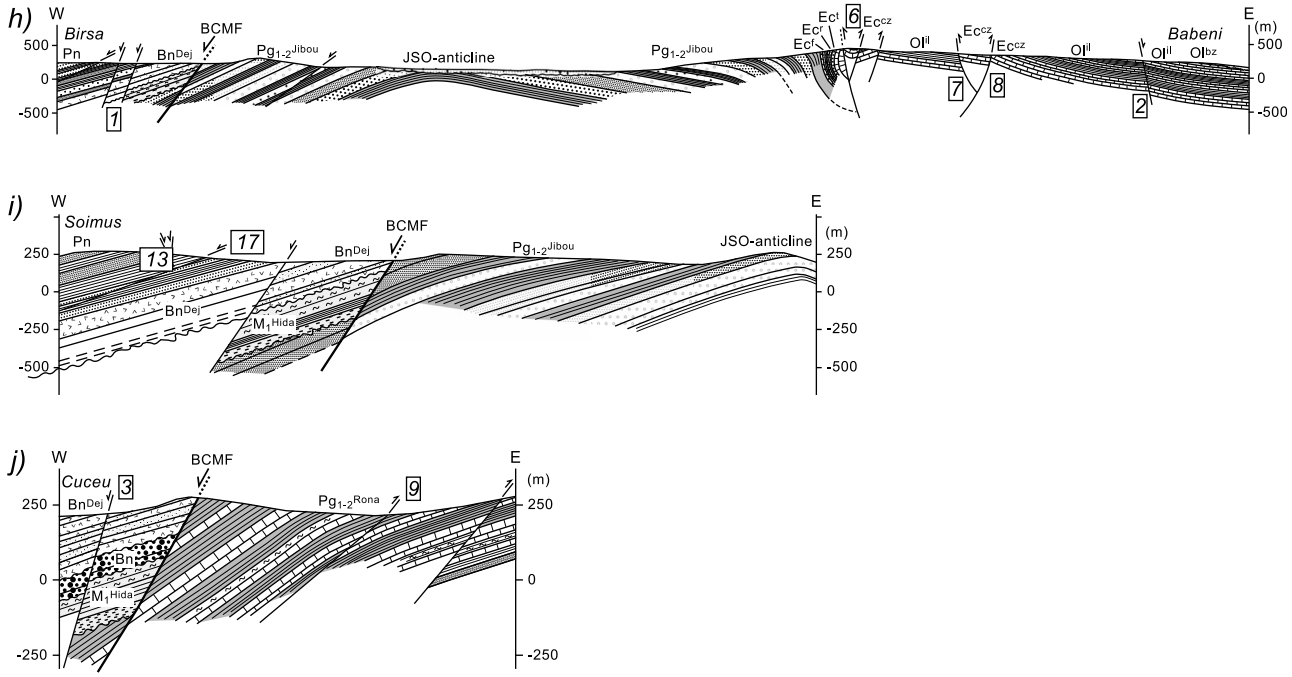

Figure 8. (continued)

[30] The MT itself is often accompanied by a wide (tens of meters) cataclastic zone of deformation developed in the hanging wall basement or Banatites [see also *Györfi et al.*, 1999]. For instance at Bociu, a quartzitic cataclastic zone is furthermore truncated by a large number of brittle faults, forming elongated zones of outcrop-scale duplexes (Figures 8g and 9b). Here, kinematic indicators demonstrate E-W to ENE-WSW shortening directions (Figure 10a; location 32). At further distance from the fault zone, numerous outcrop-scale N-S to NW-SE striking thrusts, drag-folds and high-angle reverse faults are observed in the metamorphic basement, Banatites and Paleocene–Eocene sediments (Figures 8a–8g and 10a). The kinematics of these deformation structures indicate an overall E-W to ENE-WSW shortening direction with local deviations.

[31] Timing of MT faulting can be generally constrained by the truncation of the intra-Turonian Codru/Bihor nappe contact, the truncation of the uppermost Cretaceous Banatites of the Vlădeasa Massif (Figure 7) and its sealing beneath lower Miocene sediments (Figure 8a). In more detail, the kinematics suggest two moments of contraction: a larger middle–late Eocene event was followed by reduced deformation during Oligocene times. This is indicated by the age of overturned sediments in the MT footwall, which varies from the Paleocene–lower Eocene Jibou Formation to uppermost Eocene–lowermost Oligocene Brebi Marls (Figures 8a–8g). Wherever younger Oligocene deposits crop out directly against the fault contact (between Ciumarna and Hodişu; Figure 7), strata are always sub-horizontal and indicate only small-scale faulting. The onset of lower Oligocene deposition is locally marked by a change from marine to continental alluvial conditions (Figure 8c). Furthermore, a local unconformity is observed at the base of the lower Miocene sequence (Figure 8a).

[32] The most apparent structure post-dating MT deformation is a large NNE-SSW oriented normal fault bordering the Mezeş Mountains westward (Figures 7 and 8c), which offsets strata as young as middle Miocene. Kinematics of normal fault sets demonstrates overall NW-SE extensional directions (Figure 11a; locations 4 and 21). At Dealul Pietros, small-scale NW-SE striking normal faults post-date earlier thrusts (Figures 8a, 9c, and 11a; locations 14 and 18).

[33] Other structures post-dating MT deformation are SSE-ward vergent thrusts and NNE-SSW striking folds (e.g., Figures 8b and 10a; locations 4, 11 and 20), best observed by re-folding and thrusting of the overturned upper Eocene–lowermost Oligocene section at Dealul Pietros (Figures 8a and 10a; location 10). Similar NNW-SSE to NW-SE shortening directions are suggested by outcrop-scale thrust faults (Figure 10a; locations 21, 24, and 26, Figure 11a; location 16), strike-slip/tear faults (Figure 11a; locations 30, 32 and 33) and cleavage-bedding relations (Figure 10a; location 11). Map-scale strike-slip faults dextrally offset the MT (e.g., Figure 7; north of location 23).

4.2. The Transition Between the Mezeş and Ţicău Mountains

[34] In the transition area between the Mezeş and Ţicău Mountains (Figure 7), two other important deformation structures can be recognized: the Jibou-Someş-Odorhei (JSO) anticline and the Benesat–Cuceu–Moigrad Fault (BCMF).

[35] The JSO anticline is an open N-S trending anticline with Paleocene–lower Eocene sediments in its core, which are in direct contact with the basement of the Ţicău Mountains northward (Figures 7 and 8h–8j). The eastern flank of the JSO anticline consists of deformed, but progressively less tilted Paleocene to Oligocene strata, affected by a large number of NNW-SSE to N-S striking thrusts, locally over-

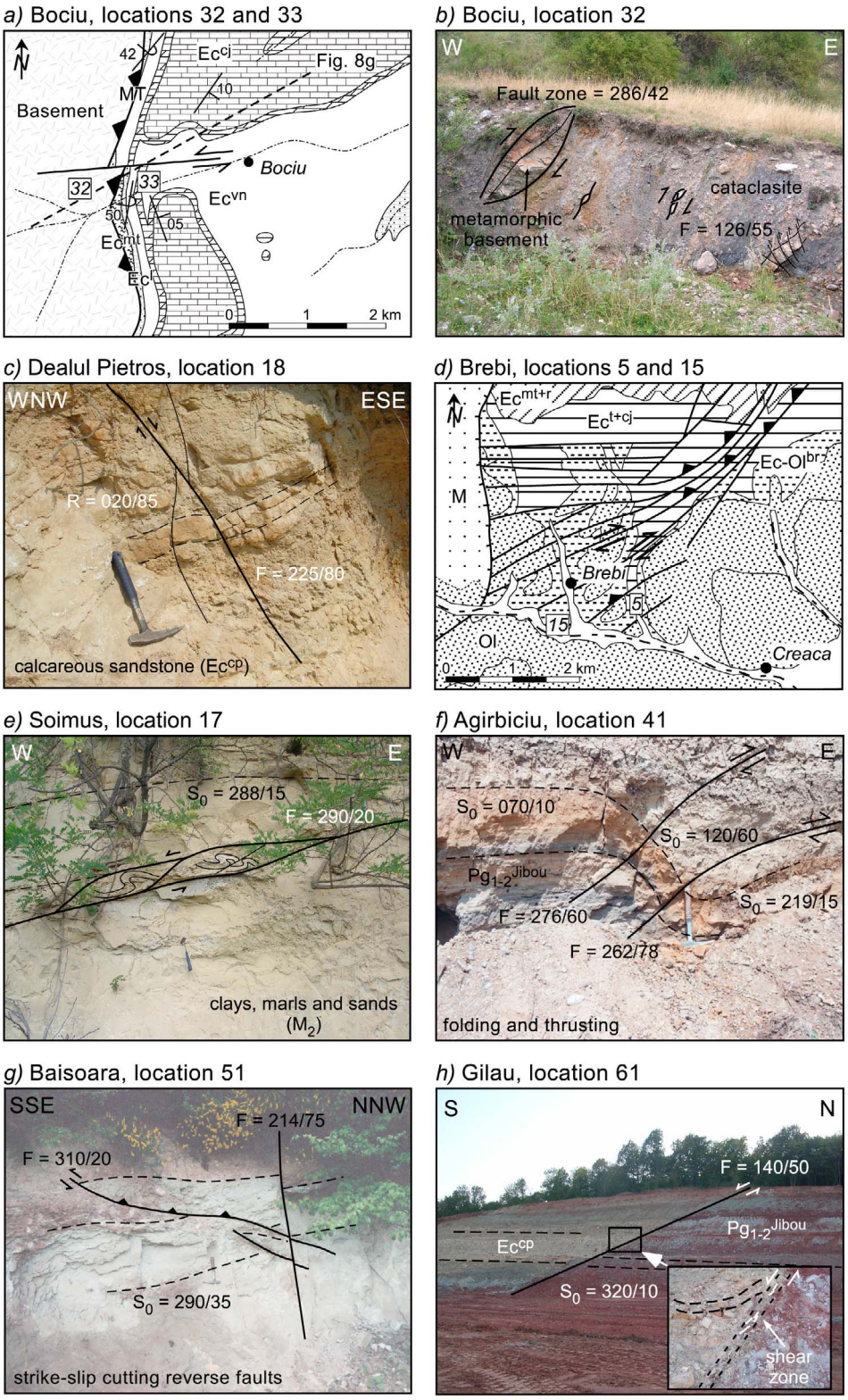

Figure 9. Field pictures and detailed maps illustrating the kinematics of the field area. Numbers in boxes represent measurement stations (see Figures 10 and 11 for locations). See Figure 2 for an explanation of abbreviations used for lithostratigraphic units. (a) Detailed map of the Bociu area. (b) Cataclasite at Bociu. (c) Normal faulting at Dealul Pietros. (d) Map of the Brebi area illustrating the change in strike of thrust faults in the transitional area between the Mezeş and Ţicău Mountains. (e) Normal faulting at Şoimus. (f) Folding and thrusting at Agîrbiciu. (g) Strike-slip faults cutting reverse faults at Baisoara. (h) Normal faulting at Gilau.

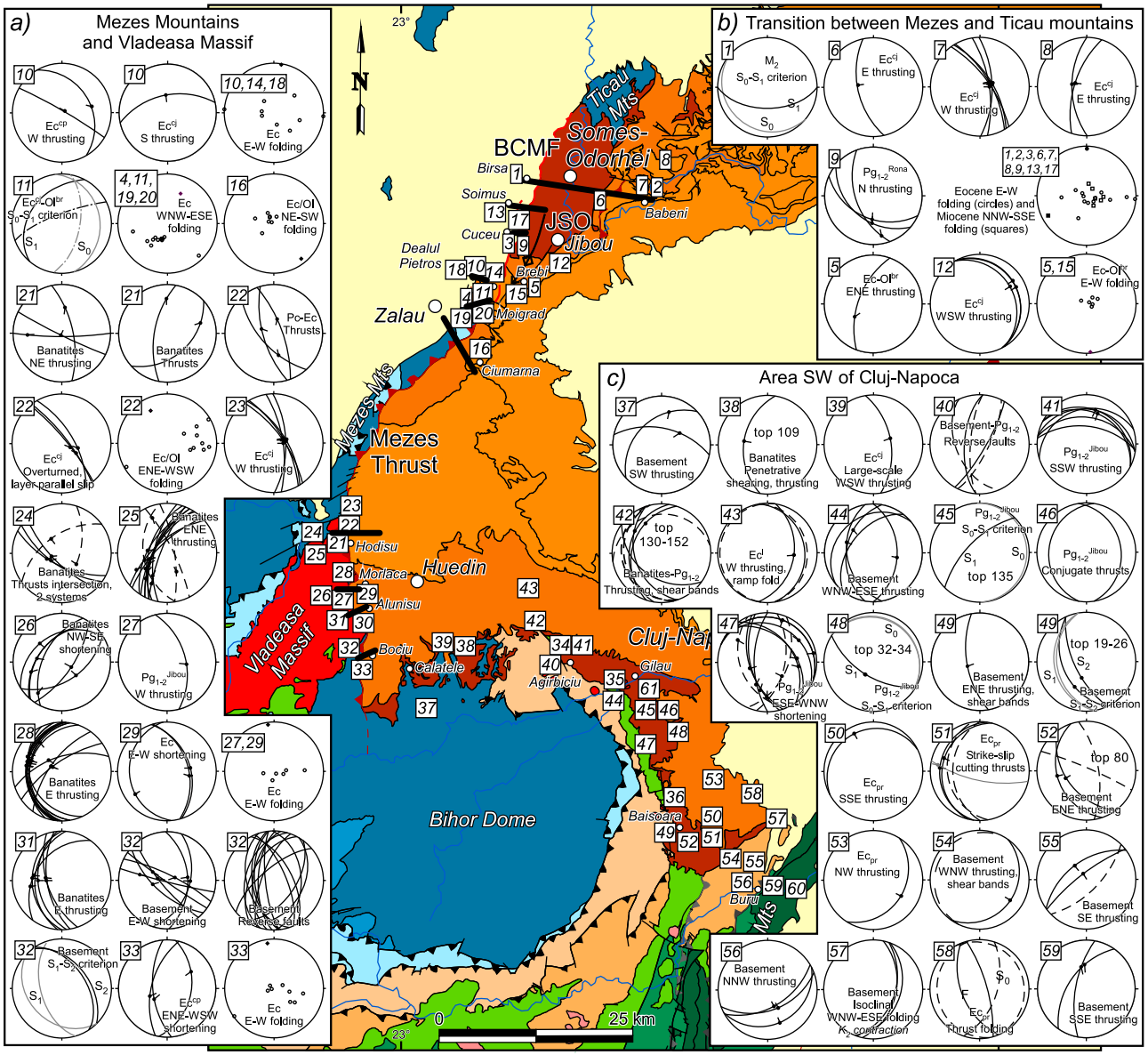

Figure 10. Overview of contractional data measured in the field (equal area stereographic projection, lower hemisphere). For stereographic projections that show orientations of bedding planes, open symbols represent poles to bedding planes and closed symbols represent the fold axes. Numbers in boxes indicate locations of measurement stations. See Figure 2 for an explanation of abbreviations used for litho-stratigraphic units. (a) Mezeş Mountains and Vlădeasa Massif. (b) Transition between Mezeş and Ţicău Mountains. (c) Area SW of Cluj-Napoca.

turning the strata and organized in pop-ups (Figures 8h and 10b; locations 6, 7 and 8). The same flank is also affected by NW-SE to ENE-WSW striking normal faults with small offsets that truncate the former set of thrusts (Figures 8h and 11b, location 2). Paleocene–lower Eocene strata are tilted up to ~40° W-wards along the western flank of the JSO anticline (Figures 8h–8j), locally affected by thrusts and high-angle reverse faults in outcrops (Figure 10b; location 9). The overall shortening direction is E-W with local strain partitioning along major structures.

[36] The overall MT offset is generally decreasing north of the Mezeş Mountains and apparently disappears near Jibou, where the fault is largely covered by Miocene sediments (Figure 7). In particular, the prolongation of the large scale deformation of the Dealul Pietros section (Figure 8a) cannot be quantified northward due to this Miocene covering. However, part of the MT offset is taken up northward toward the large scale antiform of the Ţicău Mountains by the shortening recorded in the JSO anticline and by a change in the strike of thrust faults. The latter is best observed in a series of outcrops near Brebi, where faulting in uppermost Eocene–lowermost Oligocene marls indicates a transition from low-angle NNE-SSW striking thrusts to ENE-WSW striking high-angle reverse faults with a dextral component of movement, and back to low-angle NNE-SSW striking thrusts toward the NE (Figures 9d, 10b, and 11b; locations 5, 12 and 15). These

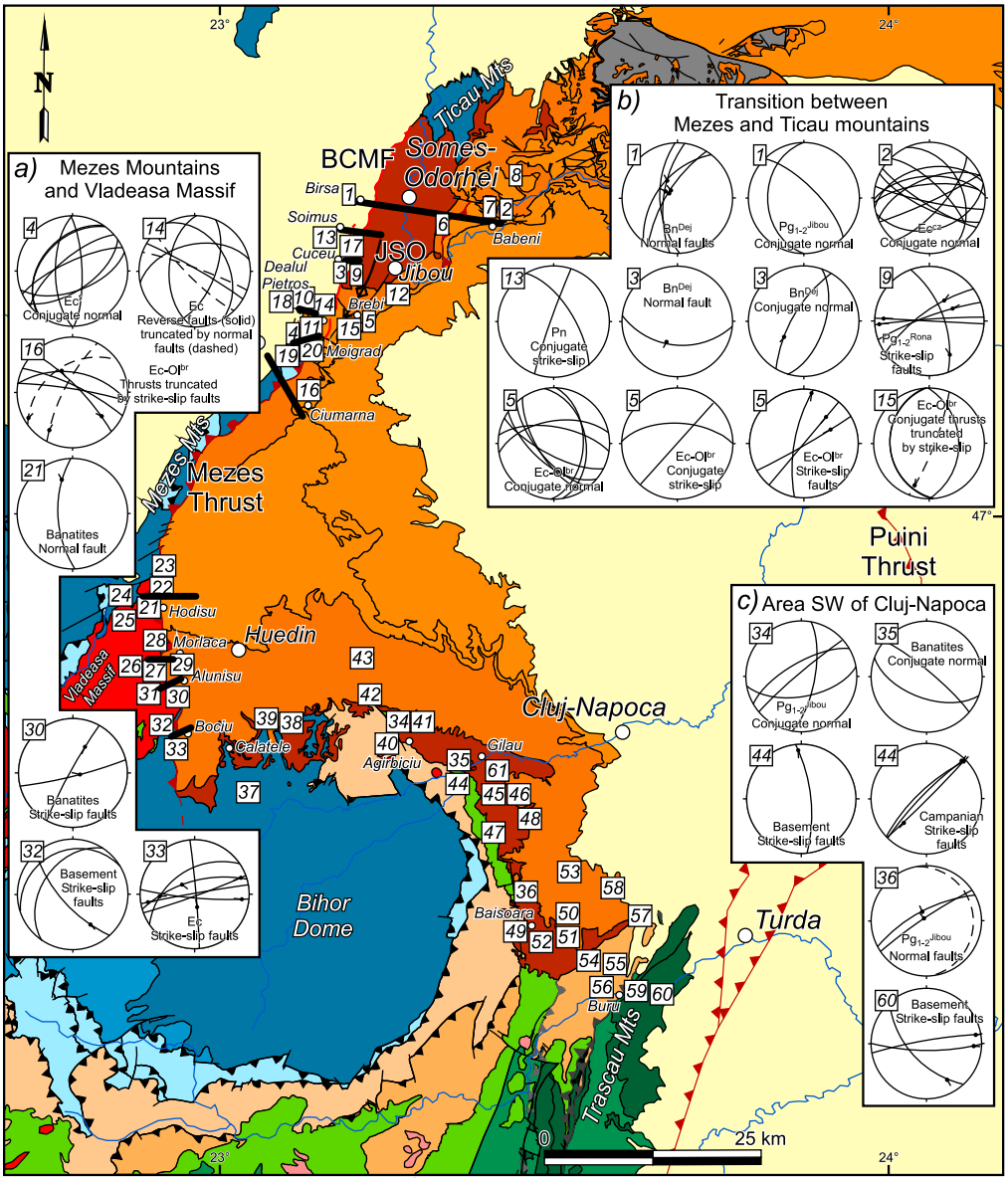

Figure 11. Overview of extensional and strike-slip data measured in the field (equal area stereographic projection, lower hemisphere), including crosscutting relation of normal and strike-slip faults with respect to reverse faults. Numbers in boxes indicate locations of measurement stations. See Figure 2 for an explanation of abbreviations used for lithostratigraphic units. (a) Mezeş Mountains and Vlădeasa Massif. (b) Transition between Mezeş and Ţicău Mountains. (c) Area SW of Cluj-Napoca.

observations support a MT offset transfer by means of a NE-ward striking transpressional duplex, accommodating local strain partitioning in a transfer zone to areas situated in the vicinity of Ţicău Mountains (Figure 7). All these faults are truncated by a large number of normal faults indicating NE-SW extension (e.g., Figure 11b; location 5), demonstrating that MT thrusting pre-dates extension.

[37] The NNE-SSW striking BCMF marks the transition between the western Pannonian area affected by large-scale (trans)tensional deformation during the Miocene and the relatively undeformed Transylvanian Basin (Figure 7). It truncates the western flank of the JSO anticline with a normal offset of up to 300 m, as inferred from stratigraphic juxtapositions against the fault (Figures 8h–8j) [see also *Popescu*, 1975]. Miocene normal faults in outcrops indicate overall E-W extension, with a rather large spread in the orientation of faults (Figures 7, 8h–8j, 9e, and 11b; locations 1, 3 and 17). Conjugate strike-slip faults (Figures 8i and 11b; location 13) and one cleavage-bedding criterion (Figure 10b; location 1) with NNE-SSW to N-S shortening directions postdate the normal faulting. The overall superposition of deformation is supported by two folding directions (E-W followed by NNW-SSE; Figure 10b) that are separated in time by the base Miocene unconformity (Figure 2).

4.3. The Area Southwest of Cluj-Napoca

[38] Paleogene sediments also crop out on the northern border of the Apuseni Mountains SW of Cluj-Napoca

(Figure 7). Although a large number of structures were observed in the field, no significant regional structures can be identified outside of the Puini thrust (Figure 7). The continental Paleocene–lower Eocene Jibou Formation (Figure 2) nonconformably covers the Cretaceous contacts of the Apuseni nappe pile, being subsequently tilted by following the morphology of the Bihor Dome. Their remnants crop out at high elevations (e.g., NE of Călatele, Figure 7; locations 38 and 39), suggesting >1000 m post-early Eocene uplift and erosion.

[39] Thrusting is frequent in the basement, Banatites and the Paleocene–Eocene sequence (Figure 10c). Map-scale NNW-SSE to N-S striking folds, thrusts and local cataclastic zones cut the basement, Banatites and Paleocene–lower Eocene deposits, showing mainly top to the east shortening directions (Figures 9f and 10c; locations 38–40, 42, 43–49, 52 and 58). These pre-date strike-slip faults with generally E-W compressional directions (Figure 11c; location 44). A second direction of contraction oriented NNE-SSW is defined by numerous E-W oriented thrusts (Figures 10c; locations 37 and 41). Closer to the Trascău Mountains, thrusting is gradually rotating to E-W and then to NW-SE shortening directions, following the structural trend of the Puini thrust system located eastward (Figures 7, 9g, and 10c; locations 50, 51, 53–57 and 59). Normal faults with dispersed directions truncate Eocene sediments, crosscutting the earlier high-angle reverse faults (Figures 9h and 11c, locations 34, 35, 36 and 61). Furthermore, E-W to NW-SE trending strike-slip faults cut the NNE-SSW trending thrusts (Figures 9g, 10c, and 11c; locations 51 and 60).

5. Late Cretaceous–Miocene Exhumation and Tectonics of the Apuseni Mountains

[40] The new AFT and AHe ages from the studied tectonic units are all Campanian and younger and therefore indicative for latest Cretaceous to present-day cooling (Figure 12). Exhumation related to older Middle–Late Jurassic, late Early Cretaceous and intra-Turonian tectonic events (Figures 13a and 13b) was recorded by higher temperature thermochronometers, as shown by Jurassic–Early Cretaceous $^{40}Ar/^{39}Ar$ (hornblende, muscovite and whole rock) ages of *Dallmeyer et al.* [1999] and intra-Turonian and older zircon fission track (partly provenance) ages of *Schuller* [2004]. The new thermochronological data, in combination with field observations and previous AFT data of *Sanders* [1998], *Schuller* [2004], and *Schuller et al.* [2009], reveal that post-collisional exhumation may have taken place rather continuously, but that it can overall be grouped in three periods: latest Cretaceous–Paleocene, middle Eocene–Oligocene and Miocene (Figure 12). Except for the Neogene volcanics, no consistent Miocene or younger cooling is indicated by the AFT and AHe ages, suggesting that post-Paleogene exhumation is restricted to less than 1 to 1.5 km of removed overburden.

5.1. Latest Cretaceous–Paleocene Exhumation: "Laramian" Thrusting and Banatitic Magmatism

[41] AFT and AHe data show a large number of latest Cretaceous–Paleocene ages for both the crystalline basement and the Banatites (Figure 12). For the Banatites, these ages are indistinguishable from $^{40}Ar/^{39}Ar$ amphibole and biotite ages [*Wiesinger et al.*, 2005], suggesting latest Cretaceous cooling of magmatic rocks to shallow depths. Thermal modeling based on the AFT and AHe data confirms cooling of the Banatites at ~50 ± 20°C/Ma between ~75–65 Ma (Figure 6a).

[42] The crystalline basement is characterized by many latest Cretaceous–Paleocene AFT ages. Since these AFT ages are also recorded in basement areas more than few tens of kilometers away from Banatite magmatism (Figure 3), it is unlikely that they are thermally affected by magmatism. It suggests that they rather record a tectonic event. Assuming a paleogeothermal gradient of 25 ± 10°C/km based on present-day regional heat-flow values of ~60 mW/m^2 [e.g., *Dövenyi and Horváth*, 1988; *Demetrescu and Andreescu*, 1994], cooling of 90 ± 57°C suggested by thermal modeling (Figure 6b) would imply 3.6 ± 2.7 km of exhumation for the crystalline basement during latest Cretaceous–Paleocene times. Based on the available data, no younger exhumation event is recorded in the crystalline basement of the Bihor Dome (Figure 12c), which suggests that its present-day topography originates from a tectonic episode that took place during latest Cretaceous–Paleocene times and that subsequent exhumation must be less than ~1.5–1.0 km in the center of the dome.

[43] The latest Cretaceous–Paleocene exhumation is younger than the late Turonian–early Coniacian "Gosau" deposition in the Apuseni Mountains (Rimeți flysch, the Lower Gosau group of *Schuller* [2004]), which can be correlated with the Late Cretaceous normal faulting observed in the vicinity of the Puini thrust (Figures 3 and 12b). However, the exhumation recorded in the basement is coeval with magmatic cooling of the Banatites and the late Campanian to Maastrichtian age of the "Laramian" tectonic event, which led to nappe emplacement in the Southern Apuseni Mountains [e.g., *Schmid et al.*, 2008, and references therein]. Campanian–Maastrichtian sediments have not been reset after deposition and yield AFT provenance ages of ~75 Ma (Figure 3; Upper Gosau group) [*Schuller*, 2004]. Short lag times and the increase in metamorphic heavy minerals indicate that they are the erosional products of the uplifting Bihor Dome during late Campanian–Maastrichtian times [*Schuller and Frisch*, 2006]. A genetic relationship between exhumation of the Bihor Dome during contraction and the coeval sedimentation is therefore obvious. Furthermore, Paleogene

Figure 12. Crustal-scale cross-sections through the Apuseni Mountains and Transylvanian Basin (2 × vertical exaggeration; see Figure 1c for locations) constructed based on seismic sections [*Krézsek and Bally*, 2006], cross-section 3 of *Schmid et al.* [2008] and 1: 200,000 geological maps of the Geological Institute of Romania. Thermochronological ages are plotted above the sections (scale-bar on the left side of the plots; see legend for explanation of symbols). Background colors in the thermochronological plots are discussed evolutionary periods, (bottom to top) Miocene-Quaternary, middle Eocene-Oligocene, latest Cretaceous–early Eocene, late Albian–Santonian and Early Cretaceous. Solid lines represent topography (25 × vertical exaggeration; scale-bar on the right side of the plots). (a) Cross-section through the Mezeş Mountains. (b) Cross-section through the Vlădeasa Massif. (c) Cross-section through the Bihor Dome.

sediments nonconformably overlying Gosau deposits record an influx of detrital material with ZFT age populations that are characteristic for the Bihor and Codru nappes [*Schuller et al.*, 2009], suggesting ongoing exposure and erosion of these units during Paleocene times possibly as a result of compressional tectonics.

[44] Further to the east, the exhumation is coeval with the main phase of thrusting/inversion observed along the Puini

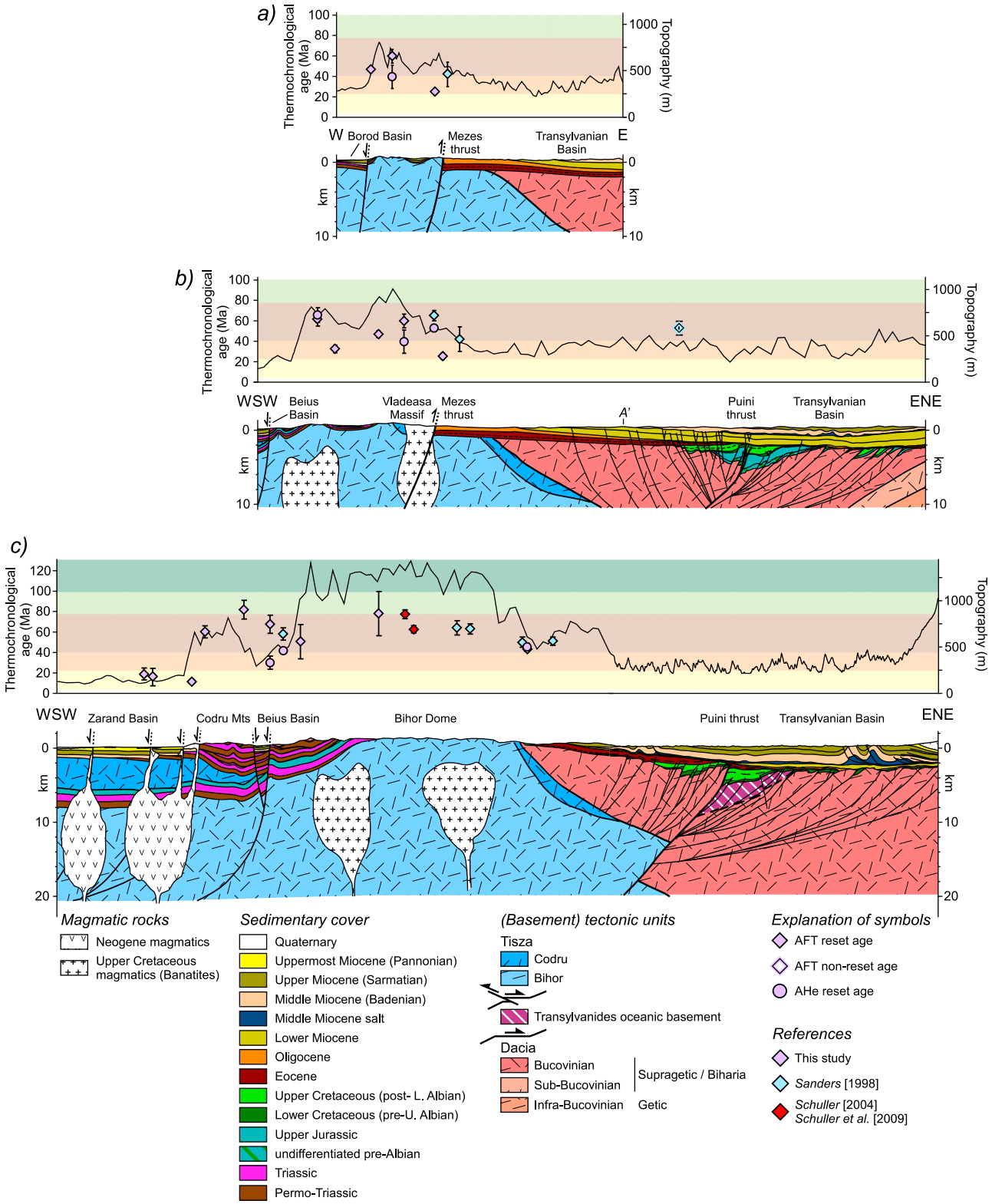

Figure 12

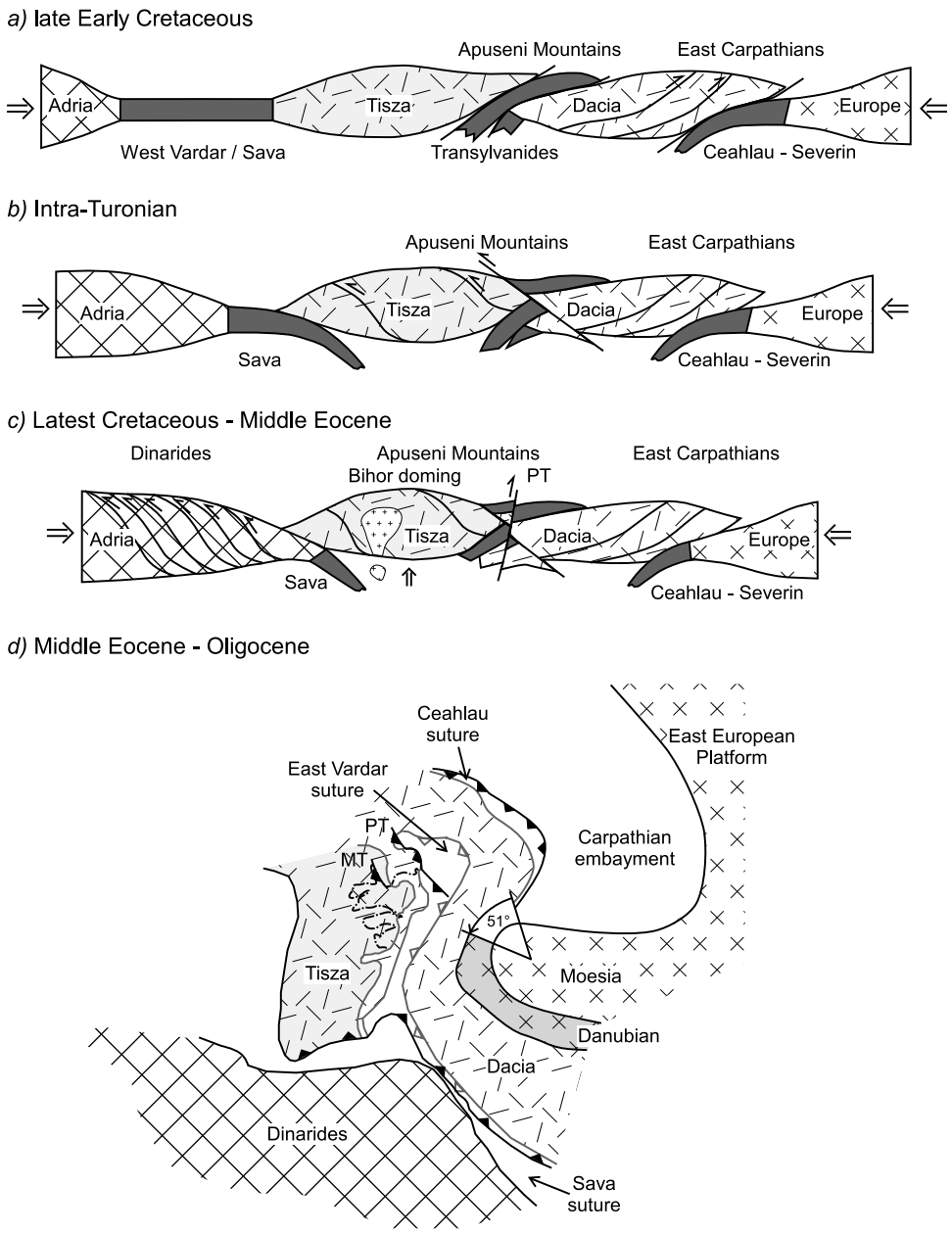

Figure 13. Schematic sketches depicting the plate tectonic evolution of the Apuseni Mountains [after *Schmid et al.*, 1998; *Schuller*, 2004; *Schmid et al.*, 2008; *Ustaszewski et al.*, 2008]. Note that the oceanic crust obducted in Late Jurassic times in the Dinarides is not displayed. (a) Late Early Cretaceous, (b) Intra-Turonian, (c) Latest Cretaceous–middle Eocene, and (d) Middle Eocene–Oligocene (reconstructed from the restored map of *Ustaszewski et al.* [2008] by a further 13° counter clockwise retro-rotation of Tisza-Dacia around Moesia [*Fügenschuh and Schmid*, 2005], amounting to a total of 51° retro-rotation for the situation at the end of the Eocene). See text for discussion.

thrust and its hanging wall erosion (Figure 12) [see also *Krézsek and Bally*, 2006] and its prolongation at the contact between the Southern Apuseni Mountains and the Transylvanian Basin (Figure 3) [*Schmid et al.*, 2008]. It is also coeval with the numerous smaller-scale thrusts observed at depth in the Transylvanian Basin (Figures 12b and 12c). A latest Maastrichtian cover seals the thick-skinned thrust contacts [e.g., *Paraschiv*, 1979; *De Broucker et al.*, 1998].

[45] Overall, it can be concluded that the latest Cretaceous–Paleocene AFT and AHe cooling ages are the combined result of a tectonic shortening and magmatic cooling event affecting the entire Apuseni Mountains (Figure 13c). No younger exhumation event is recorded in the AFT ages of the Bihor Dome flanked by the Codru nappes (Figure 12c).

[46] The genetic mechanism related to the formation of the antiformal shape of the Bihor Dome and associated E-W to NE-SW compression [see also *Schuller*, 2004] is probably a combined effect of subduction-collision tectonics of the Sava Zone and the Ceahlău-Severin Ocean (Figures 12c and 13c). The first subduction zone accommodated the Late

Cretaceous–Eocene shortening recorded in the Dinarides between the Tisza/Dacia and Adriatic continental units [*Dimitrijević*, 1997], while the second recorded the Late Cretaceous shortening between Dacia and the European units situated in its foreland [e.g., *Schmid et al.*, 2008].

[47] The large distance presently separating the Apuseni Mountains from the Dinarides is the combined result of the Miocene extension and collapse of the Pannonian basin, and the invasion and rotation of the Tisza-Dacia block into the Carpathian embayment; these areas were, however, situated in spatial proximity in pre-Miocene times [e.g., *Ustaszewski et al.*, 2008]. In addition, the Banatites are calc-alkaline subduction products of the Sava Zone (the Vardar subduction of *Zimmerman et al.* [2008]). Therefore, doming of the Bihor Dome and the observed shortening-related exhumation seems to be driven by the Sava subduction zone (Figure 13c). However, in the Southern Apuseni Mountains, the "Laramian" thrusts form large offset nappes and are presently oriented E-W [see *Balintoni*, 1994], parallel to the orientation of the latest Cretaceous nappe structure (Ceahlău-Severin related) of the South Carpathians situated in its immediate vicinity [see *Iancu et al.*, 2005] (Figure 1). Thus, at the scale of the entire Apuseni Mountains the genetic mechanism of this tectonic event is most probably a combination of the Sava and Ceahlău-Severin subduction zones.

5.2. Middle Eocene–Oligocene Exhumation: Thrusting Along the Mezeş and Puini Thrusts

[48] The thermochronological and kinematic data indicate two exhumation and deformation pulses during the Paleogene. The first pulse is of middle Eocene age (~45 Ma) and is mainly indicated by the AFT/AHe age pair of 44 ± 3/46 ± 3 Ma for Carp 100 (Table 1) and the thermal models (Figure 6). Cooling of ~85 ± 13°C between 55–40 Ma indicated by thermal modeling of the Banatites (Figure 6a) suggests 3.4 ± 1.5 km of exhumation for these samples during the middle Eocene. Samples that record middle Eocene exhumation are mainly derived from the Mezeş Mountains and Vlădeasa Massif, the northern border of the Bihor Dome, the Trascău Mountains and possibly the Biharia nappes (Figures 3 and 12).

[49] The second pulse is of early Oligocene age (~30 Ma) and is mainly indicated by the kinematic data, which show contractional structures affecting strata as young as the lowermost Oligocene. The most visible structure in map-view is the ESE-ward Mezeş thrusting over Paleocene–lower Oligocene deposits (Figure 7), with Paleocene–Eocene sediments commonly drag-folded in the footwall (Figures 8a–8g). This deformation is also responsible for widespread N-S to NNE-SSW striking thrusts, re-folded foliations and the gradual transfer zone observed at Brebi (Figures 9a and 10a). Toward the north between the Mezeş Mountains and the Ţicău Mountains, folding of the Paleocene–Eocene succession in the JSO anticline and widespread N-S oriented thrusts indicate similar E-W shortening directions (Figures 8h–8j and 10b). Southwards in the Bihor Dome, no structures can be dated as Paleogene because of the lack of coeval sediments. However, N-S oriented thrusts are observed in map-view in the prolongation of the Mezeş thrust and outcrop-scale kinematics indicates similar ENE-WSW shortening directions (Figures 7, 9f, and 10c). This second pulse is less evident in the thermochronological data, but is suggested by the AFT and AHe ages of samples from the basement, Banatites and Senonian sedimentary cover (RO-34, RO-13, RO-28 and Carp 2; Table 1) and thermal models (Figure 6). Cooling of 83 ± 46°C and 90 ± 57°C between 35–25 Ma for Banatites and basement suggests similar exhumation estimates of 3.3 ± 2.3 km to 3.6 ± 2.7 km for both units during the early Oligocene. Samples that record this early Oligocene exhumation pulse are mainly derived from the Mezeş Mountains, Vlădeasa Massif and Trascău Mountains (Figure 3). Timing of this Paleogene exhumation pulse coincides with an unconformity and the onset of the clastic Oligocene sedimentation cycle in the Transylvanian Basin (Figure 2).

[50] In the Transylvanian Basin, the latest Cretaceous Puini thrust was reactivated during the Paleogene with offsets in the order of 1–3 km (Figure 12). The gradually emergent hanging wall controlled the paleogeography during a first exhumation pulse, recorded by syn-tectonic patterns during the Paleocene-Lutetian (during deposition of the Jibou Formation), nonconformably overlain by the Bartonian–lowermost Priabonian sediments (Calata Group; Figure 2; [*De Broucker et al.*, 1998]; the "Sag 1" cycle of *Krézsek and Bally* [2006]). Near Cluj Napoca, outcrop-scale structures indicating E-W to NE-SW shortening directions are compatible with the changes in the orientation of the Puini thrust (Figure 7). This situation is strikingly similar with the smaller-scale swing of the Mezeş thrust at Brebi (Figures 7 and 9a). Here, a second phase of syn-tectonic patterns is observed, in younger upper Eocene–lowermost Oligocene sediments (Turea Group, Figure 2; the "Sag 2" cycle of *Krézsek and Bally* [2006]).

[51] The two major NNE-SSW oriented Mezeş and Puini thrusts delineate the middle Eocene–Oligocene exhumation ages (Figures 3 and 12). Combining the thermochronological and field data, the conclusion is, therefore, that the middle Eocene and early Oligocene exhumation phases are related to the shortening observed along the Mezeş and Puini thrusts (Figures 13c and 13d). The first phase is coeval with a generalized E-ward thrusting, while the second reactivation formed localized zones of offset transfer and transpressional duplexes. These two phases represent a higher-resolution interpretation of the overall ENE-WSW early Oligocene shortening previously suggested [e.g., *Györfi et al.*, 1999; *Fodor et al.*, 1999].

[52] The geodynamic driving mechanisms of these Paleogene events seem to be again a combination of contractional tectonics driven by subduction zones situated elsewhere (Figure 13d). The middle Eocene exhumation is coeval with the shortening taking place during the final moments of collision in the Dinarides (the "Dinaric" phase of *Dimitrijević* [1997]). The Paleogene exhumation events are also coeval with the initiation of Tisza-Dacia rotation around the Moesian promontory [e.g., *Balla*, 1987; *Ratschbacher et al.*, 1993; *Pătraşcu et al.*, 1994; *Márton et al.*, 2007] and the shortening taking place at the exterior of the Carpathians, as recorded by exhumation studies [*Merten et al.*, 2010].

5.3. Middle Miocene Extension

[53] Structural data from the northern part of the study area indicate significant normal faulting along and near the NNE-SSW oriented BCMF, with offsets in the order of ~300 m (Figures 7 and 8h–8j). Outcrop-scale structures show N-S to NE-SW oriented normal faults and combined with the general homogeneous orientation of conjugate normal faults (e.g., Figures 9g and 11) an overall NW-SE to WNW-ESE extensional direction can be derived.

[54] Geological maps indicate that strata as young as early Pannonian have been affected by this extensional phase [*Vlad et al.*, 1994], which combined with field observations have led to a previously assigned late Miocene age [*Györfi et al.*, 1999]. However, the new field data indicate that the youngest strata affected by normal faulting are the middle Miocene tuffs (middle Badenian), while Pannonian deposits terminate nonconformably against an inherited lineament. Therefore it is likely that the main phase of normal faulting is of middle Miocene age, compatible with the well known age of the extension in the Pannonian Basin [e.g., *Horváth et al.*, 2006], leading to the deposition of 6 km of syn- and post-rift sediments [e.g., *Tari et al.*, 1999]. This age is furthermore compatible with observations from the Transylvanian Basin, where normal faults with small offsets are observed at depth in middle Miocene (middle Badenian) sediments only [*Krézsek et al.*, 2010] or are defined by surface kinematics [*Huismans et al.*, 1997]. In this respect, the BCMF can be the most E-wards, large-scale expression of the middle Miocene normal faulting of Pannonian type. These middle Miocene tectonic events have not been recorded by low-temperature thermochronology in the Apuseni Mountains.

5.4. Late Middle to Late Miocene Deformation and Volcanism

[55] The Mezeş thrust is dextrally offset by a large number of NE-SW to ENE-WSW oriented strike-slip faults in map and outcrop scale, indicating NNW-SSE to NW-SE shortening directions (e.g., Figures 7, 9h, and 11). These faults truncate older reverse and normal faults and are recorded in sediments as young as Pannonian. Immediately NE of the study area, large-scale transcurrent movements are recorded along the WNW-ESE oriented Bogdan and Dragos Voda fault systems (Figure 1a) at 16–10 Ma, culminating with the final exhumation of the Rodna horst at 11–10 Ma [*Tischler et al.*, 2007; *Gröger et al.*, 2008]. This strike-slip phase is common in the internal areas of the Carpathians during final nappe emplacement of the external Carpathian thrust belt at ~11 Ma [e.g., *Ciulavu et al.*, 2000] and is generally related to the obliquity of shortening during collision of the East Carpathians in respect to the external European/Moesian foreland in the east (Figure 1a) [e.g., *Tischler et al.*, 2007].

[56] Neogene volcanics from the southern part of the study area have AFT ages corresponding to their Badenian–Pannonian intrusion ages of ~13–11 Ma [*Roşu et al.*, 1997; 2004; *Seghedi*, 2004]. These volcanics are intruded through NW-SE striking grabens at the western margin of the Apuseni Mountains and interpretations generally assume that magmatism is generated by decompressional melting during extension [e.g., *Balintoni and Vlad*, 1998; *Seghedi*, 2004]. This correlates with structural observations, which indicate that the onset of extension in these grabens is middle Miocene in age (i.e., ~16 Ma), but subsequent normal faulting coeval with the main collapse phase of the Pannonian Basin is also recorded in these basins during the upper part of the middle Miocene [e.g., *Dinu et al.*, 1991; *Csontos*, 1995].

5.5. Latest Miocene–Recent Exhumation: Inversion of the Transylvanian Basin

[57] The Transylvanian Basin was exhumed to sub-aerial conditions as a result of the external Carpathian collision around ~9 Ma [e.g., *Matenco et al.*, 2010]. With a later onset, accelerated subsidence of the center of the neighboring Pannonian Basin is observed starting from the Pliocene, generally interpreted as a result of folding due to Adriatic indentation, strongly influenced by local eustatic events [e.g., *Pinter et al.*, 2005; *Juhász et al.*, 2007; *Gábris and Nador*, 2007]. The Apuseni Mountains would correspond to an antiformal shape in this overall lithospheric folding geometry [*Cloetingh et al.*, 1999]. This lithospheric folding geometry [*Horváth and Cloetingh*, 1996] is not recorded by the AFT and AHe data, suggesting that post-Pannonian exhumation is less than ~1–1.5 km. This suggests that part of the topography of the Bihor Dome originates from latest Cretaceous–Paleocene times.

6. Conclusions

[58] Following the collisional tectonic events which took place during the middle part of the Cretaceous (late Early Cretaceous–Turonian), the latest Cretaceous–Tertiary evolution of the presently exposed Apuseni Mountains was mainly driven by deformation along plate boundaries exposed elsewhere in the external Carpathians or Dinarides. Thermochronological and field data indicate that the present-day topography of the Apuseni Mountains formed mainly during latest Cretaceous times, slightly modified by several tectonic pulses during the Paleogene (i.e., Mezeş and Puini thrusting).

[59] After the main late Early Cretaceous and intra-Turonian nappe stacking events, widespread latest Cretaceous–Paleocene exhumation occurred due to general doming of the Apuseni Mountains as a result of shortening and Banatitic magmatism. This was coeval with and followed by massive clastic sedimentation of the eroding Apuseni Mountains in the adjacent Transylvanian Basin. The shortening is probably driven by retro-vergent deformation of the Ceahlău-Severin Zone and by the onset of collision and associated calc-alkaline volcanism in the Sava Zone of the Dinarides (i.e., the Banatites) [see also *Schmid et al.*, 2008; *Zimmerman et al.*, 2008].

[60] Paleogene exhumation and deformation pulses can be related to regional shortening recorded along two deep-seated faults (the Mezeş and Puini thrusts) driven again by subduction processes at other plate boundaries. The first pulse can be related to the final collisional phases recorded in the Sava Zone. The Paleogene exhumation and deformation pulses are also coeval with part of the Tisza-Dacia rotation around the Moesian promontory, which is recorded in the shortening-related exhumation of the SE Carpathians [*Merten et al.*, 2010], and the orogen-parallel extension and the transcurrent movements of the South Carpathians [*Schmid et al.*, 1998]. The second pulse may be genetically related to these external Carpathian movements. The thermochronological data and the tectonostratigraphy of the Transylvanian Basin suggest that these Paleogene exhumation pulses are comparable in the order of ~3.5 km each. Paleogene exhumation contradicts the general view that this was a period of tectonic quiescence, subsidence and overall sedimentation.

[61] Middle Miocene extension and associated magmatism did not induce significant regional exhumation in the Apuseni Mountains. Estimated amounts of exhumation are near or below the resolution of the low-temperature thermochronometers.

Table A1. Apatite Fission Track Analytical Data

	Age Data[a]										Length Data[b]			
Sample Code	$N_{Gr.}$	ρ_s ($\times 10^6 cm^{-2}$)	N_s	ρ_i ($\times 10^6 cm^{-2}$)	N_i	$P(\chi^2)$ (%)	Disp.(%)	Age ± 1σ (Ma)	U (ppm)	D_{par} ± SD_{Dpar} (μm)	MTL ± 1σ (μm)	SD_L	N_L	D_{par} ± SD_{Dpar} (μm)
RO-13	21	0.288	187	0.711	462	98	0	67.5 ± 8.9	8.9	2.1 ± 0.3	15.06 ± 0.09	0.91	108	2.2 ± 0.3
RO-14	14	0.030	20	0.298	196	100	0	17.1 ± 4.4	3.3	2.3 ± 0.3	14.72 ± 0.20	0.79	15	2.1 ± 0.5
RO-15	21	0.152	66	0.557	242	5	45	54.9 ± 11.4	5.5	1.4 ± 0.2	13.42 ± 0.20	1.25	38	1.3 ± 0.1
RO-16	7	0.808	358	2.650	1174	1	18	53.5 ± 7.4	29.9	1.3 ± 0.1	14.18 ± 0.20	1.14	33	1.3 ± 0.2
RO-18	10	0.045	12	0.423	112	86	0	17.9 ± 5.7	4.9	1.7 ± 0.1	12.24 ± 0.97	1.94	4	1.8 ± 0.2
RO-20	4	0.026	4	2.776	42	97	0	15.9 ± 8.5	3.4	2.3 ± 0.4	14.68 ± 0.39	1.55	16	2.1 ± 0.4
RO-22	27	0.090	117	1.329	1735	72	1	11.3 ± 1.6	14.8	2.2 ± 0.4	15.24 ± 0.18	0.89	25	2.1 ± 0.5
RO-23	22	1.074	473	3.004	1323	<1	27	58.6 ± 7.7	33.6	1.7 ± 0.3	13.55 ± 0.19	1.28	44	1.3 ± 0.2
RO-25	15	1.424	544	2.897	1107	95	0	81.8 ± 9.2	32.2	1.6 ± 0.3	13.17 ± 0.89	2.35	7	1.6 ± 0.3
RO-27	34	0.282	667	0.765	1808	57	7	61.1 ± 6.8	8.1	1.7 ± 0.2	14.65 ± 0.11	1.01	90	1.6 ± 0.2
RO-28	28	0.233	305	1.198	1567	12	23	30.3 ± 4.0	18.1	1.7 ± 0.4	14.57 ± 0.15	1.03	46	1.6 ± 0.4
RO-31	34	0.642	521	2.084	1692	<1	27	45.9 ± 5.7	29.9	2.1 ± 0.2	13.87 ± 0.40	1.49	14	1.9 ± 0.3
RO-34	38	0.067	216	0.441	1428	82	2	25.3 ± 3.1	5.1	1.4 ± 0.3	14.09 ± 0.18	1.48	66	1.5 ± 0.2
RO-35	34	0.176	485	0.491	1356	22	14	59.4 ± 6.9	5.8	1.5 ± 0.1	14.17 ± 0.08	0.92	130	1.5 ± 0.2
RO-36	5	0.124	13	0.409	43	62	0	50.5 ± 16.7	4.7	1.2 ± 0.2	-	-	-	-
RO-37	8	0.042	22	0.089	47	93	0	78.0 ± 21.6	1.1	1.3 ± 0.3	13.37 ± 0.29	1.50	26	1.3 ± 0.1

[a] $N_{Gr.}$ is number of dated apatite crystals; ρ_s (ρ_i) are spontaneous (induced) track densities; N_s (N_i) are the number of spontaneous (induced) tracks counted; dosimeter track density (ρ_d) for this set of samples is 1.038×10^6 tracks/cm^2 with 14,642 tracks counted on the dosimeter (N_d); $P(\chi^2)$ is Chi-square (χ^2) probability [*Galbraith*, 1981]; Disp. is dispersion in single grain ages [*Galbraith and Laslett*, 1993]; Age is central age ± 1σ standard error [*Galbraith and Laslett*, 1993]; U is U-content in parts per million; D_{par} is average etch pit diameter with SD_{Dpar} its standard deviation.

[b] MTL ± 1σ is c-axis projected mean track length [*Donelick et al.*, 1999] ± 1σ standard error; SD_L is standard deviation of track length distribution; N_L is number of measured horizontal confined tracks; D_{par} is average etch pit diameter with SD_{Dpar} its standard deviation.

[62] Significant post-Pannonian exhumation would be expected during the inversion of the intra-Carpathian area related to the continental collision in the East Carpathians at ~11 Ma, or during the late stage (post 7 Ma) inversion of the Pannonian Basin during the Adriatic indentation. However, both events are not recorded in the Apuseni Mountains by the AFT and AHe thermochronometers (i.e., exhumation <1.5 km).

Appendix A: Apatite Fission Track Analysis

[63] After standard crushing, sieving, heavy liquid and magnetic separation, apatites were mounted in epoxy resin, polished and etched for 35 s in 1.6 M HNO_3 at 21°C [e.g., *Murrell et al.*, 2009]. Two mounts were prepared for each sample; one for age determinations and one for confined track length measurements. TINT fission track densities in length mounts were enhanced prior to etching using ^{252}Cf-derived fission fragment tracks [*Donelick and Miller*, 1991]. Samples were dated by external detector method with muscovite detectors [*Gleadow and Duddy*, 1981]. Mounts for age determinations were irradiated at the low-flux reactor of the ECN in Petten, the Netherlands with CN5 dosimeter glasses. After irradiation, external detectors of age mounts and dosimeter glasses were etched in 48% HF at 21°C for 12 and 25 min, respectively.

[64] Track counting and length measurements (Table A1) were performed using an Olympus BX51 optical microscope at 500 × and 1000 × magnification, respectively, equipped with an AUTOSCAN™ Systems Pty Ltd computerized microscope stage. AFT ages were determined using a zeta value [*Hurford and Green*, 1983] of 323 ± 32 for apatite and dosimeter glass CN5. Fission track ages were calculated with TRACKKEY (version 4.2.g) [*Dunkl*, 2002]. Confined track lengths were normalized for track angle using the c-axis projection model of *Donelick et al.* [1999] to increase the consistency of the measurements and to compensate for Cf-irradiation and observer bias [e.g., *Barbarand et al.*, 2003; *Ketcham*, 2005b; *Ketcham et al.*, 2007, 2009]. Etch pit diameters (D_{par}) were measured in order to constrain the kinetic characteristics of the apatite grains [*Donelick*, 1993; *Burtner et al.*, 1994; *Ketcham et al.*, 1999] (Table A1).

[65] HeFTy modeling [*Ketcham*, 2005a] of AFT data was carried out using the annealing model of *Ketcham et al.* [1999], which requires the use of the etching procedure as outlined by *Carlson et al.* [1999]. The effect of the different etching procedure used in this study was calibrated by *Murrell et al.* [2009] and would imply a maximum overestimation of 1.4–4.0°C on this data set (D_{par} values of 1.2–2.3 μm; Table A1) [see *Merten et al.*, 2010], which falls within the errors of the modeling process for these samples.

Appendix B: Apatite (U-Th)/He Analysis

[66] Inclusion-free apatite crystals were carefully hand-picked in alcohol under polarized light. Selected crystals were photographed and dimensions were measured for F_T-correction [*Farley et al.*, 1996; *Farley*, 2002]. Single crystal replicates have been analyzed for all samples (Tables B1 and B2).

[67] ^{4}He analyses were performed at the VU University Amsterdam (VUA, Table B1) and at the Scottish Universities Environmental Research Centre (SUERC, Table B2) following procedures of *Foeken et al.* [2003] and *Foeken et al.* [2006], respectively. System background ^{4}He-blanks for VUA-measurements (Table B1) yielded $6.3 \times 10^{-12} \pm 2.2 \times 10^{-12}$ ccSTP (n = 5, VUA-measurements 2005) and $4.5 \times 10^{-11} \pm 2.5 \times 10^{-11}$ ccSTP (n = 9, VUA-measurements 2008). Blanks contributed up to 82% and blank corrections have been applied (Table B1). Single crystal ages that required blank corrections > 50% have been excluded from further geological interpretations (Table B1). System background ^{4}He-blanks for SUERC measurements (Table B2) yielded $1.8 \times 10^{-12} \pm 3.1 \times 10^{-13}$ ccSTP (n = 19). Blank corrections for SUERC samples are <1% (Table B2). Re-extracts

Table B1. (U-Th)/He Analytical Data VUA-Measurements

Sample Code	^{4}He[c] (ccSTP)	^{4}He Blank Correction	^{238}U[c] (ng)	^{238}U Blank Correction	^{232}Th[c] (ng)	^{232}Th Blank Correction	Th/U	eU[d] (ppm)	Uncorrected Age (Ma)	F_T[e]	Corrected Age (Ma)
Carp 92p1[a]	1.20E-10	5%	0.018	5%	0.046	2%	2.6	17	34.2 ± 1.8	0.62	54.8 ± 7.5
Carp 92p2[a]	1.50E-10	4%	0.019	5%	0.062	2%	3.3	25	36.5 ± 1.7	0.59	61.4 ± 10.8
Carp 92p3[a]	1.88E-10	3%	0.026	3%	0.075	1%	2.9	14	35.0 ± 1.4	0.69	50.9 ± 4.1
Error weighted average Carp 92											52.8 ± 3.4
RO-13p1[b]	1.28E-10	26%	0.035	1%	0.066	1%	1.9	23	20.8 ± 4.6	0.61	34.0 ± 7.9
RO-13p2[b,f]	3.77E-11	54%	0.011	4%	0.035	2%	3.3	11	16.0 ± 10.6	0.61	26.3 ± 17.4
RO-13p3[b]	4.95E-11	47%	0.017	3%	0.050	2%	3.0	11	14.2 ± 7.2	0.65	21.9 ± 11.1
RO-13p4[b,f]	9.73E-12	82%	0.010	4%	0.031	3%	3.2	12	4.7 ± 11.9	0.58	8.1 ± 20.6
Error weighted average RO-13											29.9 ± 6.5
RO-22p1[b,g]	3.44E-10	11%	0.010	4%	0.017	4%	1.8	4	200.9 ± 21.2	0.71	283.7 ± 34.2
RO-22p2[b,g]	1.11E-10	29%	0.055	1%	0.006	3%	0.1	26	16.3 ± 4.2	0.67	24.3 ± 6.9
RO-22p3[b,f]	2.72E-11	62%	0.007	6%	0.006	12%	0.9	6	28.1 ± 25.9	0.61	46.5 ± 42.9
Error weighted average RO-22											-
RO-27p1[b]	2.63E-10	15%	0.031	1%	0.094	1%	3.1	9	40.4 ± 4.9	0.73	55.1 ± 9.8
RO-27p2[b]	3.77E-10	11%	0.031	1%	0.126	1%	4.1	12	50.7 ± 4.6	0.72	70.7 ± 22.7
RO-27p3[b]	2.92E-10	13%	0.014	3%	0.144	1%	10.6	18	49.9 ± 4.9	0.65	76.3 ± 20.5
RO-27p4[b]	1.54E-10	22%	0.012	4%	0.045	2%	3.8	9	55.9 ± 9.6	0.68	81.9 ± 14.8
Error weighted average RO-27											65.6 ± 7.2
RO-28p1[b,g]	1.17E-10	28%	0.009	5%	0.023	3%	2.7	6	68.1 ± 15.1	0.65	105.1 ± 28.0
RO-28p2[b,g]	2.49E-10	15%	0.012	4%	0.033	2%	2.9	8	105.4 ± 12.2	0.67	157.7 ± 21.7
RO-28p3[b,g]	6.37E-11	41%	0.007	6%	0.022	4%	3.0	9	41.6 ± 16.4	0.60	69.9 ± 29.7
Error weighted average RO-28											-
RO-34p1[b,f]	2.76E-11	62%	0.012	4%	0.001	48%	0.1	4	18.9 ± 17.1	0.70	27.0 ± 24.5
RO-34p2[b,f]	1.87E-11	71%	0.002	20%	B.D.	100%	-	1	84.5 ± 113.8	0.70	120.0 ± 162.4
RO-34p3[b,f]	4.68E-11	49%	0.012	4%	0.001	59%	0.0	4	32.9 ± 17.6	0.68	48.3 ± 26.9
Error weighted average RO-34											-
RO-35p1[b,f]	4.93E-11	48%	0.016	3%	B.D.	72%	-	7	25.1 ± 12.9	0.67	37.6 ± 19.8
RO-35p2[b,f]	1.35E-10	25%	0.011	4%	B.D.	100%	-	6	96.8 ± 20.2	0.63	152.9 ± 36.3
RO-35p3[b,f]	1.02E-10	30%	0.009	5%	B.D.	100%	-	4	94.7 ± 25.9	0.67	141.3 ± 39.4
RO-35p4[b]	7.74E-11	37%	0.023	2%	0.002	32%	0.1	11	26.9 ± 8.9	0.66	40.4 ± 13.8
Error weighted average RO-35											40.4 ± 13.8
VU Durango Fluorapatite											
Durango 6[a]	2.99E-09	0%	0.122	1%	2.551	0%	21.5		34.0 ± 1.1		
Durango 1[b]	2.01E-09	2%	0.069	1%	1.753	0%	26.0		34.2 ± 1.7		
Durango 2[b]	1.80E-09	2%	0.075	1%	1.545	0%	21.2		33.7 ± 1.6		
Durango 3[b]	2.66E-09	2%	0.100	0%	2.339	0%	24.1		33.6 ± 1.6		
Average ± standard deviation									33.9 ± 0.3		

[a]VUA-measurements 2005 following procedures of *Foeken et al.* [2003]. ^{4}He abundances were calibrated against an internal standard with a reproducibility of 1.1% (1σ, n = 16, May-June 2005). Following He-extraction, apatites were prepared for U and Th analyses following procedures of *Foeken et al.* [2003] and spiked with a calibrated ^{229}Th/^{233}U solution.

[b]VUA-measurements 2008 following procedures of *Foeken et al.* [2003]. ^{4}He abundances were calibrated against an internal standard with a reproducibility of 0.6% (1σ, n = 12, March 2008). Following He-extraction, apatites were prepared for U and Th analyses following procedures of *Foeken et al.* [2003] and spiked with a calibrated ^{229}Th/^{233}U solution.

[c]Blank corrected values; B.D., below detection limit.

[d]Effective uranium concentration, where eU = U + 0.235 × Th [*Shuster et al.*, 2006; *Flowers et al.*, 2007].

[e]Corrected ages are corrected for α-ejection using the model for a hexagonal prism geometry; F_T is fraction of α retained [*Farley et al.*, 1996].

[f]Not taken into account for error weighted average because of >50% blank/sample ratio.

[g]Not taken into account for error weighted average.

were routinely run for each sample, and were all within system background levels.

[68] Following Helium extraction, apatites were prepared for U and Th analyses following procedures of *Foeken et al.* [2003] (VUA samples) and *Balestrieri et al.* [2005] (SUERC samples) and spiked with a calibrated ^{229}Th/^{233}U solution. Instrument- and full procedure blanks were measured to assess ^{238}U and ^{232}Th background levels. VUA samples of 2008 yielded full procedure blanks of 0.4 ± 0.1 pg and 0.8 ± 0.3 pg (^{238}U and ^{232}Th respectively, n = 5). These samples generally required ^{238}U and ^{232}Th blank corrections of <10%, occasionally up to 100% (Table B1). Single crystal ages that required blank corrections > 50% have been excluded from further geological interpretations (Table B1). VUA samples of 2005 yielded full procedure blanks of 0.9 ± 0.9 pg and 1.1 ± 0.7 pg (^{238}U and ^{232}Th respectively, n = 4), requiring blank corrections of <5% for ^{238}U and <2% for ^{232}Th (Table B1). Full procedure blanks for SUERC samples yielded 0.9 ± 0.1 pg and 6.0 ± 0.6 pg (^{238}U and ^{232}Th respectively, n = 2), thus generally requiring blank corrections of <6% (Table B2).

[69] Reported 1σ errors on single crystal ages (Tables B1 and B2) are propagated from the analytical uncertainties of ^{238}U, ^{232}Th and ^{4}He determinations and blank corrections, and the uncertainty of the F_T-correction. Analytical errors generally are ~3–6% for VUA-2005 and SUERC samples and ~10–30% for VUA-2008 samples. The uncertainty of the F_T-correction has been assessed by repeated length and diameter determinations of all crystals and is usually in the order of 2–15%, occasionally up to 30%. For each sample the error weighted average of single crystal ages has been calculated, which has subsequently been used for further interpretation (Tables B1 and B2).

Table B2. (U-Th)/He Analytical Data SUERC-Measurements[a]

Sample Code	^{4}He[b] (ccSTP)	^{4}He Blank Correction	^{238}U[b] (ng)	^{238}U Blank Correction	^{232}Th[b] (ng)	^{232}Th Blank Correction	Th/U	eU[c] (ppm)	Uncorrected Age (Ma)	F_T[d]	Corrected Age (Ma)
Carp 97p1[e]	3.45E-10	1%	0.027	3%	0.014	30%	0.5	13	93.7 ± 3.5	0.65	143.1 ± 21.6
Carp 97p2[e]	3.56E-10	1%	0.045	2%	0.017	26%	0.4	16	59.4 ± 2.3	0.66	90.5 ± 18.8
Carp 97p3[e]	2.99E-10	1%	0.025	3%	0.014	31%	0.6	22	86.0 ± 3.3	0.61	140.5 ± 18.2
Error weighted average Carp 97											-
Carp 100p1	5.08E-10	0%	0.101	1%	0.151	4%	1.5	105	30.5 ± 1.1	0.68	44.6 ± 4.6
Carp 100p2	7.21E-10	0%	0.115	1%	0.145	4%	1.3	64	39.7 ± 1.4	0.72	55.4 ± 5.4
Carp 100p3	6.92E-10	0%	0.168	1%	0.223	3%	1.4	119	25.8 ± 0.9	0.72	35.9 ± 6.3
Error weighted average Carp 100											46.0 ± 3.0
Carp 105p1	1.94E-10	1%	0.042	2%	0.107	5%	2.6	39	23.6 ± 0.8	0.61	38.6 ± 2.6
Carp 105p2	2.16E-10	1%	0.038	2%	0.096	6%	2.6	30	29.2 ± 1.1	0.64	45.8 ± 3.5
Carp 105p3	2.67E-10	1%	0.045	2%	0.153	4%	3.5	49	27.1 ± 1.0	0.60	45.3 ± 4.3
Error weighted average Carp 105											42.0 ± 1.9
					VU Durango Fluorapatite						
Durango D11	8.90E-10	0%	0.044	2%	0.773	1%	18.0		32.3 ± 1.7		
Durango D13	1.43E-09	0%	0.063	1%	1.216	0%	19.7		33.5 ± 1.4		
Durango D1	1.13E-09	0%	0.042	2%	1.023	1%	25.1		32.7 ± 1.4		
Durango D2	2.33E-09	0%	0.097	1%	2.078	0%	22.0		32.6 ± 1.4		
Average ± standard deviation									32.8 ± 0.6		

[a]SUERC-measurements following procedures of *Foeken et al.* [2006]. ^{4}He concentrations were calculated by peak height comparison against a calibrated standard with a reproducibility of 1.4% (1σ, n = 46, July-August 2006). Following He-extraction, apatites were prepared for U and Th measurements following procedures of *Balestrieri et al.* [2005] and spiked with a calibrated ^{229}Th/^{233}U solution.
[b]Blank corrected values.
[c]Effective uranium concentration, where eU = U + 0.235 × Th [*Shuster et al.*, 2006; *Flowers et al.*, 2007].
[d]Corrected ages are corrected for α-ejection using the model for a hexagonal prism geometry; FT is fraction of α retained [*Farley et al.*, 1996].
[e]Not taken into account for error weighted average.

[70] VU Durango fluorapatites (60–180 μm, 1 to 3 fragments) were analyzed in order to verify analytical procedures and age calibrations. VUA Durango ages are 33.9 ± 0.3 Ma (n = 4; Table B1) and SUERC Durango ages are 32.8 ± 0.6 Ma (n = 4; Table B2), which is in good agreement with previously reported AHe ages (e.g., 32.1 ± 1.7 Ma [*House et al.*, 2000], 32.0 ± 1.0 Ma [*Farley*, 2002]).

[71] HeFTy modeling [*Ketcham*, 2005a] of AHe data was carried out using the *Farley* [2000] Durango He-diffusion model. Whereas more recent diffusion models [e.g., *Shuster et al.*, 2006; *Flowers et al.*, 2009] have become available, the *Farley* [2000] diffusion model is justified for these samples as they generally have low eU concentrations (Tables B1 and B2) and have been cooled rapidly (suggesting that alpha-radiation is of minor importance) [e.g., *Shuster et al.*, 2006].

[72] **Acknowledgments.** This research forms part of the Pannonian–Carpathian program of the Netherlands Research Centre for Integrated Solid Earth Science (ISES). F. Stuart is thanked for the AHe analyses carried out at SUERC. R. van Elsas, T. Vogel-Eissens, J. Juez-Larré, D. Vilbert and B. van der Wagt are thanked for assistance in mineral separation procedures, fission track preparation, and He, U and Th analyses. S. Schmid and B. Fügenschuh are acknowledged for discussions on the kinematics of the Apuseni Mountains and earlier versions of this manuscript. F. Neubauer and an anonymous reviewer are thanked for their constructive reviews, which significantly improved the manuscript.

References

Angelier, J. (1994), Fault slip analysis and palaeostress reconstruction, in *Continental Deformation*, edited by P. L. Hancock, pp. 53–100, Pergamon, Oxford, U. K.

Balestrieri, M. L., F. M. Stuart, C. Persano, E. Abbate, and G. Bigazzi (2005), Geomorphic development of the escarpment of the Eritrean margin, southern Red Sea from combined apatite fission-track and (U–Th)/He thermochronometry, *Earth Planet. Sci. Lett.*, *231*, 97–110, doi:10.1016/j.epsl.2004.12.011.

Balintoni, I. (1994), Structure of the Apuseni Mountains, *Rom. J. Tectonics Reg. Geol.*, *75*, suppl. 2, 51–58.

Balintoni, I., and Ş. Vlad (1998), Tertiary magmatism in the Apuseni Mountains and related tectonic setting, *Stud. Univ. Babes Bolyai, Geol. Geogr.*, *9*, 1–11.

Balla, Z. (1987), Tertiary paleomagnetic data for the Carpatho-Pannonian region in the light of Miocene rotation kinematics, *Tectonophysics*, *139*, 67–98, doi:10.1016/0040-1951(87)90198-3.

Barbarand, J., T. Hurford, and A. Carter (2003), Variation in apatite fission-track length measurement: Implications for thermal history modelling, *Chem. Geol.*, *198*, 77–106, doi:10.1016/S0009-2541(02)00423-0.

Batt, G. E., and M. T. Brandon (2002), Lateral thinking: 2-D interpretation of thermochronology in convergent orogenic settings, *Tectonophysics*, *349*, 185–201, doi:10.1016/S0040-1951(02)00053-7.

Berza, T., E. Constantinescu, and S. Vlad (1998), Upper Cretaceous magmatic series and associated mineralisation in the Carpathian-Balkan orogen, *Resour. Geol.*, *48*(4), 291–306, doi:10.1111/j.1751-3928.1998.tb00026.x.

Bleahu, M., M. Lupu, D. Patrulius, S. Bordea, A. Ştefan, and S. Panin (1981), *The Structure of the Apuseni Mountains: Guide to Excursion B3*, *Guideb. Ser.*, vol. 23, translated from Romanian, 107 pp., Inst. of Geol. and Geophys., Bucharest.

Burtner, R. L., A. Nigrini, and R. A. Donelick (1994), Thermochronology of Lower Cretaceous source rocks in the Idaho–Wyoming thrust belt, *AAPG Bull.*, *78*(10), 1613–1636.

Carlson, W. D., R. A. Donelick, and R. A. Ketcham (1999), Variability of apatite fission-track annealing kinetics: I. Experimental results, *Am. Mineral.*, *84*, 1213–1223.

Ciulavu, D. (1999), Tertiary tectonics of the Transylvanian Basin, Ph.D. thesis, 152 pp., Vrije Univ., Amsterdam.

Ciulavu, D., C. Dinu, A. Szakacs, and D. Dordea (2000), Neogene kinematics of the Transylvanian Basin (Romania), *AAPG Bull.*, *84*(10), 1589–1615.

Ciulavu, D., C. Dinu, and S. A. P. L. Cloetingh (2002), Late Cenozoic tectonic evolution of the Transylvanian Basin and northeastern part of the Pannonian Basin (Romania): Constraints from seismic profiling and numerical modeling, in *Neotectonics and Surface Processes: The Pannonian Basin and Alpine-Carpathian System*, *Stephan Mueller Spec. Publ. Ser.*, vol. 3, edited by S. A. P. L. Cloetingh et al., pp. 105–120, Eur. Geosci. Union, Munich, Germany.

Cloetingh, S., E. Burov, and A. Poliakov (1999), Lithosphere folding: Primary response to compression? (from central Asia to Paris basin), *Tectonics*, *18*, 1064–1083, doi:10.1029/1999TC900040.

Csontos, L. (1995), Tertiary tectonic evolution of the Intra-Carpathian area: A review, *Acta Vulcanol.*, *7*(2), 1–13.

Csontos, L., and A. Vörös (2004), Mesozoic plate tectonic reconstruction of the Carpathian region, *Palaeogeogr. Palaeoclimatol. Palaeoecol.*, *210*(1), 1–56, doi:10.1016/j.palaeo.2004.02.033.

Csontos, L., E. Márton, G. Worum, and I. Benkovics (2002), Geodynamics of SW-Pannonian inselbergs (Mecsek and Villány Mts, SW Hungary): Inference from complex structural analysis, in *Neotectonics and Surface Processes: The Pannonian Basin and Alpine-Carpathian System*, *Stephan Mueller Spec. Publ. Ser.*, vol. 3, edited by S. A. P. L. Cloetingh et al., pp. 1–19, Eur. Geosci. Union, Munich, Germany.

Dallmeyer, R. D., D. I. Pana, F. Neubauer, and P. Erdmer (1999), Tectonothermal evolution of the Apuseni Mountains, Romania: Resolution of Variscan versus Alpine events with $^{40}Ar/^{39}Ar$ ages, *J. Geol.*, *107*, 329–352, doi:10.1086/314352.

De Broucker, G., A. Mellin, and P. Duindam (1998), Tectono-stratigraphic evolution of the Transylvanian Basin, pre-salt sequence, Romania, *Bucharest Geosci. Forum Spec. Vol.*, *1*, 36–69.

Demetrescu, C., and M. Andreescu (1994), On the thermal regime of some tectonic units in a continental collision environment in Romania, *Tectonophysics*, *230*, 265–276, doi:10.1016/0040-1951(94)90140-6.

Dimitrijević, M. D. (1997), Geology of Yugoslavia, 2nd ed., 187 pp., Geol. Inst. Gemini, Belgrade.

Dinu, C., C. Calota, V. Mocanu, and D. Ciulavu (1991), Geotectonic setting and the particular structural features of the Beius basin, on the basis of geological and geophysical data synthesis, *Rev. Roum. Geol., Geophys. Geogr., Geophys.*, *35*, 77–87.

Donelick, R. A. (1993), Apatite etching characteristics versus chemical composition, *Nucl. Tracks Radiat. Meas.*, *21*, 604, doi:10.1016/1359-0189(93)90241-Z.

Donelick, R. A., and D. S. Miller (1991), Enhanced TINT fission track densities in low spontaneous track density apatites using ^{252}Cf-derived fission fragment tracks: A model and experimental observations, *Nucl. Tracks Radiat. Meas.*, *18*, 301–307, doi:10.1016/1359-0189(91)90022-A.

Donelick, R. A., R. A. Ketcham, and W. D. Carlson (1999), Variability of apatite fission-track annealing kinetics II: Crystallographic orientation effects, *Am. Mineral.*, *84*, 1224–1234.

Dövenyi, P., and F. Horváth (1988), A review of temperature, thermal conductivity and heat flow data from the Pannonian Basin, *AAPG Mem.*, *45*, 195–233.

Dunkl, I. (2002), Trackkey: A Windows program for calculation and graphical presentation of fission track data, *Comput. Geosci.*, *28*, 3–12, doi:10.1016/S0098-3004(01)00024-3.

Ehlers, T. A., and K. A. Farley (2003), Apatite (U–Th)/He thermochronometry: Methods and applications to problems in tectonics and surface processes, *Earth Planet. Sci. Lett.*, *206*, 1–14, doi:10.1016/S0012-821X(02)01069-5.

Farley, K. A. (2000), Helium diffusion from apatite: General behavior as illustrated by Durango fluorapatite, *J. Geophys. Res.*, *105*(B2), 2903–2914, doi:10.1029/1999JB900348.

Farley, K. A. (2002), (U-Th)/He dating: Techniques, calibrations, and applications, in *Noble Gases in Geochemistry and Cosmochemistry*, *Rev. Mineral. Geochem.*, vol. 47, edited by D. Porcelli, C. J. Ballentine, and R. Wieler, pp. 819–843, Mineral. Soc. of Am., Washington, D. C., doi:10.2138/rmg.2002.47.18.

Farley, K. A., R. A. Wolf, and L. T. Silver (1996), The effects of long alpha-stopping distances on (U-Th)/He ages, *Geochim. Cosmochim. Acta*, *60*, 4223–4229, doi:10.1016/S0016-7037(96)00193-7.

Filipescu, S. (2001), Cenozoic lithostratigraphic units in Transylvania, in *Algae and Carbonate Platforms in Western Part of Romania*, edited by I. I. Bucur, S. Filipescu, and E. Săsăran, pp. 75–92, Cluj Univ. Press, Cluj-Napoca, Romania.

Flowers, R. M., D. L. Shuster, B. P. Wernicke, and K. A. Farley (2007), Radiation damage control on apatite (U-Th)/He dates from the Grand Canyon region, Colorado Plateau, *Geology*, *35*, 447–450, doi:10.1130/G23471A.1.

Flowers, R. M., R. A. Ketcham, D. L. Shuster, and K. A. Farley (2009), Apatite (U-Th)/He thermochronometry using a radiation damage accumulation and annealing model, *Geochim. Cosmochim. Acta*, *73*, 2347–2365, doi:10.1016/j.gca.2009.01.015.

Fodor, L., L. Csontos, G. Bada, I. Györfi, and L. Benkovics (1999), Tertiary tectonic evolution of the Pannonian Basin system and neighbouring orogens: A new synthesis of palaeostress data, *Geol. Soc. Spec. Publ.*, *156*, 295–334.

Foeken, J., T. Dunai, G. Bertotti, and P. Andriessen (2003), Late Miocene to Present exhumation in the Ligurian Alps (SW Alps) with evidence for accelerated denudation during the Messinian Salinity Crisis, *Geology*, *31*, 797–800, doi:10.1130/G19572.1.

Foeken, J. P. T., F. M. Stuart, K. J. Dobson, C. Persano, and D. Vilbert (2006), A diode laser system for heating minerals for (U-Th)/He chronometry, *Geochem. Geophys. Geosyst.*, *7*, Q04015, doi:10.1029/2005GC001190.

Fügenschuh, B., and S. M. Schmid (2005), Age and significance of core complex formation in a very curved orogen: Evidence from fission track studies in the South Carpathians (Romania), *Tectonophysics*, *404*, 33–53, doi:10.1016/j.tecto.2005.03.019.

Gábris, G., and A. Nador (2007), Long-term fluvial archives in Hungary: Response of the Danube and Tisza rivers to tectonic movements and climatic changes during the Quaternary: A review and new synthesis, *Quat. Sci. Rev.*, *26*(22–24), 2758–2782, doi:10.1016/j.quascirev.2007.06.030.

Galbraith, R. F. (1981), On statistical models for fission track counts, *Math. Geol.*, *13*(6), 471–478, doi:10.1007/BF01034498.

Galbraith, R. F., and G. M. Laslett (1993), Statistical models for mixed fission track ages, *Nucl. Tracks Radiat. Meas.*, *21*, 459–470, doi:10.1016/1359-0189(93)90185-C.

Gallagher, K., R. Brown, and C. Johnson (1998), Fission track analysis and its applications to geological problems, *Annu. Rev. Earth Planet. Sci.*, *26*, 519–572, doi:10.1146/annurev.earth.26.1.519.

Gleadow, A. J. W., and I. R. Duddy (1981), A natural long-term annealing experiment for apatite, *Nucl. Tracks Radiat. Meas.*, *5*, 169–174.

Gradstein, F. M., and J. G. Ogg (2004), *A Geologic Time Scale 2004*, 589 pp., Cambridge Univ. Press, Cambridge, U. K.

Gröger, H. R., B. Fügenschuh, M. Tischler, S. M. Schmid, and J. P. T. Foeken (2008), Tertiary cooling and exhumation history in the Maramures area (internal eastern Carpathians, northern Romania): Thermochronology and structural data, *Geol. Soc. Spec. Publ.*, *298*, 169–195, doi:10.1144/SP298.9.

Györfi, I., L. Csontos, and A. Nagymarosy (1999), Early Tertiary structural evolution of the border zone between the Pannonian and Transylvanian Basins, *Geol. Soc. Spec. Publ.*, *156*, 251–267.

Haas, J., and C. Pero (2004), Mesozoic evolution of the Tisza Mega-unit, *Int. J. Earth Sci.*, *93*, 297–313, doi:10.1007/s00531-004-0384-9.

Harrison, T. M. (1981), Diffusion of ^{40}Ar in hornblende, Contrib. Mineral. Petrol., 78, 324–331, doi:10.1007/BF00398927.

Harrison, T. M., I. Duncan, and I. McDougall (1985), Diffusion of ^{40}Ar in biotite: Temperature, pressure and compositional effects, *Geochim. Cosmochim. Acta*, *49*, 2461–2468, doi:10.1016/0016-7037(85)90246-7.

Horváth, F., and S. Cloetingh (1996), Stress-induced late-stage subsidence anomalies in the Pannonian basin, *Tectonophysics*, *266*, 287–300, doi:10.1016/S0040-1951(96)00194-1.

Horváth, F., G. Bada, P. Szafián, G. Tari, A. Adam, and S. Cloetingh (2006), Formation and deformation of the Pannonian Basin: Constraints from observational data, in *European Lithosphere Dynamics*, *Geol. Soc. London Mem.*, vol. 32, edited by D. G. Gee and R. A. Stephenson, pp. 191–206, Geol. Soc., London, doi:10.1144/GSL.MEM.2006.032.01.11.

Hosu, A. (1999), Arhitectura sedimentației depozitelor Eocene din nord-vestul Depresiunii Transilvaniei, Ph.D. thesis, 224 pp., Univ. Clujeană, Cluj-Napoca Romania.

House, M. A., K. A. Farley, and D. Stockli (2000), Helium chronometry of apatite and titanite using Nd-YAG laser heating, *Earth Planet. Sci. Lett.*, *183*, 365–368, doi:10.1016/S0012-821X(00)00286-7.

Huismans, R. S., G. Bertotti, D. Ciulavu, C. A. E. Sanders, S. Cloetingh, and C. Dinu (1997), Structural evolution of the Transylvanian Basin (Romania): A sedimentary basin in the bend of the Carpathians, *Tectonophysics*, *272*, 249–268, doi:10.1016/S0040-1951(96)00261-2.

Hurford, A. J., and P. F. Green (1983), The Zeta age calibration of fission-track dating, *Chem. Geol.*, *41*, 285–317.

Iancu, V., T. Berza, A. Seghedi, I. Gheuca, and H.-P. Hann (2005), Alpine polyphase tectono-metamorphic evolution of the South Carpathians: A new overview, *Tectonophysics*, *410*, 337–365, doi:10.1016/j.tecto.2004.12.038.

Ionescu, C., V. Hoeck, C. Tomek, F. Koller, I. Balintoni, and L. Beşuțiu (2009), New insights into the basement of the Transylvanian Depression (Romania), *Lithos*, *108*, 172–191, doi:10.1016/j.lithos.2008.06.004.

Juhász, G., G. Pogácsás, I. Magyar, and G. Vakarcs (2007), Tectonic versus climatic control on the evolution of fluvio-deltaic systems in a lake basin, Eastern Pannonian Basin, *Sediment. Geol.*, *202*, 72–95, doi:10.1016/j.sedgeo.2007.05.001.

Ketcham, R. A. (2005a), Forward and inverse modeling of low-temperature thermochronology data, in *Low Temperature Thermochronology: Techniques, Interpretations, and Applications*, *Rev. Mineral. Geochem.*, vol. 58, edited by P. W. Reiners and T. A. Ehlers, pp. 275–314, Mineral. Soc. of Am., Washington, D. C., doi:10.2138/rmg.2005.58.11.

Ketcham, R. A. (2005b), The role of crystallographic angle in characterizing and modelling apatite fission-track length data, *Radiat. Meas.*, *39*, 595–601, doi:10.1016/j.radmeas.2004.07.008.

Ketcham, R. A., R. A. Donelick, and W. D. Carlson (1999), Variability of apatite fission-track annealing kinetics: III. Extrapolation to geological time scales, *Am. Mineral.*, *84*, 1235–1255.

Ketcham, R. A., A. Carter, R. A. Donelick, J. Barbarand, and A. J. Hurford (2007), Improved measurement of fission-track annealing in apatite using c-axis projection, *Am. Mineral.*, *92*, 789–798, doi:10.2138/am.2007.2280.

Ketcham, R. A., R. A. Donelick, M. L. Balestrieri, and M. Zattin (2009), Reproducibility of apatite fission-track length data and thermal history reconstruction, *Earth Planet. Sci. Lett.*, *284*, 504–515, doi:10.1016/j.epsl.2009.05.015.

Kirstein, L. A., M. G. Fellin, S. D. Willett, A. Carter, Y. G. Chen, J. I. Garver, and D. C. Lee (2010), Pliocene onset of rapid exhumation in Taiwan during arc-continent collision: New insights from detrital thermochronometry, *Basin Res.*, *22*(3), 270–285, doi:10.1111/j.1365-2117.2009.00426.x.

Kissling, E., S. M. Schmid, R. Lippitsch, J. Ansorge, and B. Fügenschuh (2006), Lithosphere structure and tectonic evolution of the Alpine arc: New evidence from high-resolution teleseismic tomography, in *European Lithosphere Dynamics*, *Geol. Soc. London Mem.*, vol. 32, edited by D. G. Gee and R. A. Stephenson, pp. 129–145, Geol. Soc., London, doi:10.1144/GSL.MEM.2006.032.01.08.

Krézsek, C., and A. Bally (2006), The Transylvanian Basin (Romania) and its relation to the Carpathian fold and thrust belt: Insights in gravitational salt tectonics, *Mar. Pet. Geol.*, *23*, 405–442, doi:10.1016/j.marpetgeo.2006.03.003.

Krézsek, C., and S. Filipescu (2005), Middle to Late Miocene sequence stratigraphy of the Transylvanian Basin (Romania), *Tectonophysics*, *410*, 437–463, doi:10.1016/j.tecto.2005.02.018.

Krézsek, C., S. Filipescu, L. Silye, L. Matenco, and H. Doust (2010), Miocene facies associations and sedimentary evolution of the Southern Transylvanian Basin (Romania): Implications for hydrocarbon exploration, *Mar. Pet. Geol.*, *27*, 191–214, doi:10.1016/j.marpetgeo.2009.07.009.

Laubscher, H. (1971), Das Alpen-Dinariden-Problem und die Palinspastik der südlichen Tethys, *Geol. Rundsch.*, *60*, 813–833, doi:10.1007/BF02046522.

Lippitsch, R., E. Kissling, and J. Ansorge (2003), Upper mantle structure beneath the Alpine orogen from high-resolution teleseismic tomography, *J. Geophys. Res.*, *108*(B8), 2376, doi:10.1029/2002JB002016.

Lippolt, H. J., M. Leitz, R. S. Wernicke, and B. Hagedorn (1994), (Uranium + thorium)/helium dating of apatite: Experience with samples from different geochemical environments, *Chem. Geol.*, *112*, 179–191, doi:10.1016/0009-2541(94)90113-9.

Márton, E., M. Tischler, L. Csontos, B. Fügenschuh, and S. Schmid (2007), The contact zone between the ALCAPA and Tisza-Dacia mega-tectonic units of Northern Romania in the light of new paleomagnetic data, *Swiss J. Geosci.*, *100*, 109–124, doi:10.1007/s00015-007-1205-5.

Matenco, L., C. Krézek, S. Merten, S. Schmid, S. Cloetingh, and P. Andriessen (2010), Characteristics of collisional orogens with low topographic build-up: An example from the Carpathians, *Terra Nova*, *22*, 155–165, doi:10.1111/j.1365-3121.2010.00931.x.

Merten, S., L. Matenco, J. P. T. Foeken, F. M. Stuart, and P. A. M. Andriessen (2010), From nappe stacking to out-of-sequence postcollisional deformations: Cretaceous to Quaternary exhumation history of the SE Carpathians assessed by low-temperature thermochronology, *Tectonics*, *29*, TC3013, doi:10.1029/2009TC002550.

Murrell, G. R., E. R. Sobel, B. Carrapa, and P. Andriessen (2009), Calibration and comparison of etching techniques for apatite fission-track thermochronology, *Geol. Soc. Spec. Publ.*, *324*, 73–85, doi:10.1144/SP324.6.

Paraschiv, D. (1979), *Romanian Oil and Gas Fields*, *Tech. Econ. Stud., Ser. A*, vol. 13, 382 pp., Inst. of Geol. and Geophys., Bucharest.

Pătraşcu, S., C. Panaiotu, M. Seclăman, and C. E. Panaiotu (1994), Timing of rotational motion of Apuseni Mountains (Romania): Paleomagnetic data from Tertiary magmatic rocks, *Tectonophysics*, *233*, 163–176, doi:10.1016/0040-1951(94)90239-9.

Pécskay, Z., O. Edelstein, I. Seghedi, A. Szakács, J. Leza, M. Kovacs, M. Crihan, and A. Bernard (1995), K-Ar datings of Neogene–Quaternary calc-alkaline volcanic rocks in Romania, *Acta Vulcanol.*, *7*, 53–61.

Petrescu, I., and D. Drăghici (1964), Cluj, in *Geological Map of Romania, L-34-XII*, sheet 10, scale 1:200,000, Geol. Inst. of Rom., Bucharest.

Petrescu, I., and C. Grigorescu (1974), Ciucea, in *Geological Map of Romania, L-34-46-B*, sheet 41b, scale 1:50,000, Geol. Inst. of Rom., Bucharest.

Petrescu, I., G. Enea, and V. Vlad (1975), Jibou, in *Geological Map of Romania, L-34-35-B*, scale 1:50,000, sheet 29b, Geol. Inst. of Rom., Bucharest.

Pinter, N., G. Grenerczy, J. Weber, S. Stein, and D. Medak (Eds.) (2005), *The Adria Microplate: GPS Geodesy, Tectonics and Hazards, NATO Science Series*, vol. 4, *Earth and Environmental Sciences*, 413 pp., Springer, Dordrecht, Netherlands.

Popescu, B. M. (1984), Lithostratigraphy of cyclic continental to marine Eocene deposits in NW Transylvania, Romania, *Arch. Sci.*, *37*, 37–73.

Popescu, G. (1975), Etudes des foraminiferes du Miocene inferieur et moyen du nord-ouest de la Transylvanie, *Mem. Inst. Geol. Geofiz.*, *23*, 5–121.

Proust, J. N., and A. Hosu (1996), Sequence stratigraphy and paleogene tectonic evolution of the Transylvanian Basin (Romania, eastern Europe), *Sediment. Geol.*, *105*, 117–140, doi:10.1016/0037-0738(95)00144-1.

Ratschbacher, L., H.-G. Linzer, F. Moser, R.-O. Strusievicz, H. Bedelean, N. Har, and P.-A. Mogos (1993), Cretaceous to Miocene thrusting and wrenching along the central south Carpathians due to a corner effect during collision and orocline formation, *Tectonics*, *12*, 855–873, doi:10.1029/93TC00232.

Reiners, P. W., and M. T. Brandon (2006), Using thermochronology to understand orogenic erosion, *Annu. Rev. Earth Planet. Sci.*, *34*, 419–466, doi:10.1146/annurev.earth.34.031405.125202.

Rögl, F. (1996), Stratigraphic correlation of the Paratethys Oligocene and Miocene, *Mitt. Ges. Geol. Bergbaustud. Oesterr.*, *41*, 65–73.

Roşu, E., Z. Pécskay, A. Ştefan, G. Popescu, C. Panaiotu, and C. E. Panaiotu (1997), The evolution of Neogene volcanism in the Apuseni Mountains (Romania), constraints from new K-Ar data, *Geol. Carpathica*, *48*(6), 353–359.

Roşu, E., I. Seghedi, H. Downes, D. H. M. Alderton, A. Szakács, Z. Pécskay, C. Panaiotu, C. E. Panaiotu, and L. Nedelcu (2004), Extension-related Miocene calc-alkaline magmatism in the Apuseni Mountains, Romania: Origin of magmas, *Schweiz. Mineral. Petrogr. Mitt.*, *84*, 153–172.

Sanders, C. A. E. (1998), Tectonics and erosion–Competitive forces in a compressive orogen: A fission track study of the Romanian Carpathians, Ph.D. thesis, 204 pp., Vrije Univ., Amsterdam.

Săndulescu, M. (1984), *Geotectonica României (GeoTectonics of Romania)*, 450 pp., Tehnicã, Bucharest.

Săndulescu, M. (1988), Cenozoic tectonic history of the Carpathians, *AAPG Mem.*, *45*, 17–25.

Săndulescu, M., and M. Visarion (1978), Considérations sur la structure tectonique du soubassement de la dépression de Transsylvanie, *Dari Seama Sedintelor Inst. Geol. Geofiz.*, *64*, 153–173.

Săndulescu, M., et al. (1978), *Geological Map of Romania*, scale 1:1,000,000, Geol. Inst. of Rom., Bucharest.

Schmid, S. M., O. A. Pfiffner, N. Froitzheim, G. Schonborn, and E. Kissling (1996), Geophysical-geological transect and tectonic evolution of the Swiss-Italian Alps, *Tectonics*, *15*, 1036–1064, doi:10.1029/96TC00433.

Schmid, S. M., T. Berza, V. Diaconescu, N. Froitzheim, and B. Fügenschuh (1998), Orogen-parallel extension in the southern Carpathians, *Tectonophysics*, *297*, 209–228, doi:10.1016/S0040-1951(98)00169-3.

Schmid, S. M., D. Bernoulli, B. Fügenschuh, L. Matenco, S. Schefer, R. Schuster, M. Tischler, and K. Ustaszewski (2008), The Alpine-Carpathian-Dinaridic orogenic system: Correlation and evolution of tectonic units, *Swiss J. Geosci.*, *101*, 139–183, doi:10.1007/s00015-008-1247-3.

Schuller, V. (2004), Evolution and geodynamic significance of the Upper Cretaceous Gosau basin in the Apuseni Mountains (Romania), Ph.D. thesis, 112 pp., Inst. für Geowissenschaften, Univ. of Tübingen, Tübingen, Germany.

Schuller, V., and W. Frisch (2006), Heavy mineral provenance and paleocurrent data of the Upper Cretaceous Gosau succession of the Apuseni Mountains (Romania), *Geol. Carpathica*, *57*(1), 29–39.

Schuller, V., W. Frisch, M. Danišík, I. Dunkl, and M. C. Melinte (2009), Upper Cretaceous Gosau deposits of the Apuseni Mountains (Romania)–Similarities and differences to the Eastern Alps, *Aust. J. Earth Sci.*, *102*, 133–145.

Seghedi, I. (2004), Geological evolution of the Apuseni Mountains with emphasis on the Neogene magmatism–A review, in *Au-Ag-telluride Deposits of the Golden Quadrilateral, Apuseni Mountains, Romania: Guidebook of the International Field Workshop of IGCP Project 486*, *IAGOD Guideb. Ser.*, vol. 11, edited by N. J. Cook and C. L. Ciobanu, pp. 5–23, Geol. Inst. of Romania, Bucharest.

Shuster, D. L., R. M. Flowers, and K. A. Farley (2006), The influence of natural radiation damage on helium diffusion kinetics in apatite, *Earth Planet. Sci. Lett.*, *249*, 148–161, doi:10.1016/j.epsl.2006.07.028.

Simpson, C., and S. M. Schmid (1983), An evaluation of criteria to deduce the sense of movement in sheared rocks, *Geol. Soc. Am. Bull.*, *94*, 1281–1288, doi:10.1130/0016-7606(1983)94<1281:AEOCTD>2.0.CO;2.

Spiegel, C., B. Kohn, D. Belton, Z. Berner, and A. Gleadow (2009), Apatite (U–Th–Sm)/He thermochronology of rapidly cooled samples: The effect of He implantation, *Earth Planet. Sci. Lett.*, *285*, 105–114, doi:10.1016/j.epsl.2009.05.045.

Ştefănescu, M., et al. (1988), Section Biharia–Malu Mare, in *Geological Cross Sections*, *Rep. 5-B*, scale 1:200,000, Geol. Inst. of Rom., Bucharest.

Tari, G., P. Dövenyi, I. Dunkl, F. Horváth, L. Lenkey, M. Ştefănescu, P. Szafian, and T. Toth (1999), Lithosphere structure of the Pannonian Basin derived from seismic, gravity and geothermal data, *Geol. Soc. Spec. Publ.*, *156*, 215–250.

Tischler, M., H. R. Gröger, B. Fügenschuh, and S. M. Schmid (2007), Miocene tectonics of the Maramures area (northern Romania): Implications for the Mid-Hungarian fault zone, *Int. J. Earth Sci.*, *96*, 473–496, doi:10.1007/s00531-006-0110-x.

Ustaszewski, K., S. Schmid, B. Fügenschuh, M. Tischler, E. Kissling, and W. Spakman (2008), A map-view restoration of the Alpine-Carpathian-Dinaridic system for the Early Miocene, *Swiss J. Geosci.*, *101*, 273–294, doi:10.1007/s00015-008-1288-7.

Vlad, V., and T. Romanoschi (1987), Răchițele, in *Geological Map of Romania*, *L-34-46-D*, sheet 41d, scale 1:50,000, Geol. Inst. of Rom., Bucharest.

Vlad, V., A. Tușinschi, and A. Stan (1994), Zalău, in *Geological Map of Romania*, *L-34-35-A*, sheet 29a, scale 1:50,000, Geol. Inst. of Rom., Bucharest.

Vlaicu-Tătărîm, N. (1963), *Stratigrafia Eocenului din Reguinea de la Sud-Vest de Cluj*, Editura Acad. Repub. Pop. Rom., Bucharest.

Wiesinger, M., F. Neubauer, T. Berza, R. Handler, and J. Genser (2005), $^{40}Ar/^{39}Ar$ amphibole and biotite dating of Romanian Banatites, paper presented at 7th Workshop on Alpine Geological Studies, 3rd Croatian Geological Congress, Croatian Geol. Surv., Opatija, Croatia, 29 Sept.–1 Oct.

Willett, S. D., and M. T. Brandon (2002), On steady states in mountain belts, *Geology*, *30*, 175–178, doi:10.1130/0091-7613(2002)030<0175:OSSIMB>2.0.CO;2.

Willingshofer, E., F. Neubauer, and S. Cloetingh (1999), The significance of Gosau-type basins for the Late Cretaceous tectonic history of the Alpine-Carpathian Belt, *Phys. Chem. Earth, Part A*, *24*, 687–695, doi:10.1016/S1464-1895(99)00100-3.

Wolf, R. A., K. A. Farley, and D. M. Kass (1998), Modeling of the temperature sensitivity of the apatite (U–Th)/He thermochronometer, *Chem. Geol.*, *148*, 105–114, doi:10.1016/S0009-2541(98)00024-2.

Zimmerman, A., H. J. Stein, J. L. Hannah, D. Koželj, K. Bogdanov, and T. Berza (2008), Tectonic configuration of the Apuseni-Banat-Timok-Srednogorie belt, Balkans-South Carpathians, constrained by high precision Re-Os molybdenite ages, *Miner. Deposita*, *43*, 1–21, doi:10.1007/s00126-007-0149-z.

P. A. M. Andriessen and S. Merten, Department of Isotope Geochemistry, Faculty of Earth and Life Sciences, Vrije Universiteit, De Boelelaan 1085, Amsterdam NL-1081 HV, Netherlands. (sandra.merten@falw.vu.nl)

J. P. T. Foeken, Research and Technology Department, Qatar Petroleum, P.O. Box 3212, Doha, Qatar.

L. Matenco, Department of Tectonics, Faculty of Earth and Life Sciences, Vrije Universiteit, De Boelelaan 1085, Amsterdam NL-1081 HV, Netherlands.